CONCEPTUAL DESIGN OF INTEGRATED ENERGY SYSTEMS VIA MULTISCALE MARKET SIMULATIONS AND SURROGATE MODELS FOR MARKET INTERACTIONS

XINHE CHEN, RADHAKRISHNA TUMBALAM GOOTY, DARICE GUITTET, BERNARD KNUEVEN, JOHN SIIROLA, JAFFER GHOUSE, ALEXANDER DOWLING, DAVID C. MILLER

GRID
MODERNIZATION LABORATORY CONSORTIUM
U.S. Department of Energy

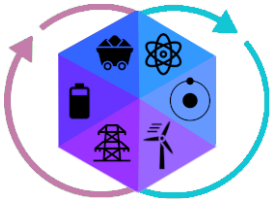

DISPATCHES
Design Integration and Synthesis Platform to Advance Tightly Coupled Hybrid Energy Systems

November 29, 2023

Disclaimers

This project was funded by the United States Department of Energy, National Energy Technology Laboratory, in part, through a site support contract. Neither the United States Government nor any agency thereof, nor any of their employees, nor the support contractor, nor any of their employees, makes any warranty, express or implied, or assumes any legal liability or responsibility for the accuracy, completeness, or usefulness of any information, apparatus, product, or process disclosed, or represents that its use would not infringe privately owned rights. Reference herein to any specific commercial product, process, or service by trade name, trademark, manufacturer, or otherwise does not necessarily constitute or imply its endorsement, recommendation, or favoring by the United States Government or any agency thereof. The views and opinions of authors expressed herein do not necessarily state or reflect those of the United States Government or any agency thereof.

Sandia National Laboratories is a multimission laboratory managed and operated by National Technology & Engineering Solutions of Sandia, LLC, a wholly owned subsidiary of Honeywell International Inc., for the U.S. Department of Energy's National Nuclear Security Administration under contract DE-NA0003525.

This manuscript has been authored by employees of Lawrence Berkeley National Laboratory under Contract No. DE-AC02-05CH11231 with the U.S. Department of Energy. The U.S. Government retains, and the publisher, by accepting the article for publication, acknowledges, that the U.S. Government retains a non-exclusive, paid-up, irrevocable, world-wide license to publish or reproduce the published form of this manuscript, or allow others to do so, for U.S. Government purposes.

This work was authored in part by the National Renewable Energy Laboratory, operated by Alliance for Sustainable Energy, LLC, for the U.S. Department of Energy (DOE) under Contract No. DE-AC36-08GO28308. Funding provided by U.S. Department of Energy Office of Energy Efficiency and Renewable Energy Solar Energy Technologies Office. The views expressed herein do not necessarily represent the views of the DOE or the U.S. Government.

Xinhe Chen[1]*: Conceptualization, Methodology, Software, Writing – Original Draft, Formal Analysis, Visualization;* ***Radhakrishna Tumbalam Gooty***[2,3]*: Conceptualization, Methodology, Software, Writing – Original Draft, Formal Analysis, Visualization;* ***Darice Guittet***[4]*: Conceptualization, Methodology, Software, Writing – Original Draft, Formal Analysis, Visualization;* ***Bernard Knueven***[4]*: Conceptualization, Software, Writing – Review & Editing, Formal Analysis;* ***John Siirola***[5]*: Conceptualization, Writing – Review & Editing, Supervision;* ***Jaffer Ghouse***[2,3]*: Conceptualization, Writing – Review & Editing, Supervision;* ***Alexander Dowling***[1]*: Conceptualization, Writing – Review & Editing, Formal Analysis, Supervision;* ***David Miller***[2*]*: Conceptualization, Writing – Review & Editing, Supervision.*

[1]*Department of Chemical and Biomolecular Engineering, University of Notre Dame, Notre Dame, IN.*
[2]National Energy Technology Laboratory (NETL), Pittsburgh, PA.
[3]NETL support contractor, Pittsburgh, PA.
[4]National Renewable Energy Laboratory, Golden, CO.
[5]Sandia National Laboratories, Albuquerque, NM.
*Corresponding contact: d.c.miller.phd@gmail.com

Acknowledgements:

This work was conducted as part of the Design Integration and Synthesis Platform to Advance Tightly Coupled Hybrid Energy Systems (DISPATCHES) project through the Grid Modernization Lab Consortium with funding from the U.S. Department of Energy's Office of Fossil Energy and Carbon Management, Office of Nuclear Energy, and Hydrogen and Fuel Cell Technology Office.

Suggested Citation:
X. Chen, R. Tumbalam Gooty, D. Guittet, B. Knueven, J. Siirola, J. Ghouse, A. Dowling, and D. Miller, "Conceptual Design of Integrated Energy Systems via Multiscale Market Simulations and Surrogate Models for Market Interactions," National Energy Technology Laboratory, Pittsburgh, November 29, 2023.

DISPATCHES TEAM

National Energy Technology Laboratory
David Miller, Jaffer Ghouse[1,2], Andrew Lee[1], Radhakrishna Tumbalam Gooty[1], Naresh Susarla[1], Andres Joaquin Calderon Vergara[1,2]

Sandia National Laboratories
John Siirola, Darryl Melander, Edna Soraya Rawlings, Kyle Skolfield, Jordan Jalving[2]

Lawrence Berkeley National Laboratory
Dan Gunter, Oluwamayowa Amusat, Keith Beattie, Ludovico Bianchi

National Renewable Energy Laboratory
Wesley Jones, Darice Guittet, Benard Knueven, Ignas Satkauskas, Abinet Eseye[2]

Idaho National Laboratory
Aaron Epiney, Joshua Cogliati, Andrea Alfonsi[2], Konor Frick[2], Jason Hansen, Cristian Rabiti[2], Jakub Toman, Elizabeth K. Worsham, Ramon K. Yoshiura, Gabriel J. Soto Gonzalez, Richa K. Sabharwall

University of Notre Dame
Alexander Dowling, Xinhe Chen, Xian Gao[2]

[1]*NETL Support Contractor*
[2]Contributed to the project but the person is no longer affiliated with the organization.

Conceptual Design of Integrated Energy Systems via Multiscale Market Simulations and Surrogate Models for Market Interactions

Xinhe Chen[1], Radhakrishna Tumbalam Gooty[2,3], Darice Guittet[4], Bernard Knueven[4], John Siirola[5], Jaffer Ghouse[2,3], Alexander Dowling[1], and David C. Miller[2]

[1]Department of Chemical and Biomolecular Engineering, University of Notre Dame, Notre Dame, IN.
[2]National Energy Technology Laboratory, Pittsburgh, PA.
[3]NETL Support Contractor, Pittsburgh, PA.
[4]National Renewable Energy Laboratory, Golden, CO.
[5]Sandia National Laboratories, Albuquerque, NM.

Executive Summary

This report demonstrates novel capabilities developed as part of DISPATCHES, Design Integration and Synthesis Platform to Advance Tightly Coupled Hybrid Energy Systems, for designing *hybrid energy systems* (HES) a.k.a. *integrated energy systems* (IES) in the context of a larger electricity market. IES combine two or more energy technologies to improve flexibility and energy efficiency, reduce carbon emissions, and improve overall grid operation, e.g., reliability. Common IES examples include generators hybridized with a large-scale energy storage system and co-generation systems that produce power and alternate products (e.g., hydrogen). IES are quite effective in responding to volatile grid conditions caused by the increasing penetration of variable renewable energy (VRE) sources in the grid. However, designing IES is challenging since the optimal design and operation depend strongly on the grid behavior, such as dispatchability, prices, etc. Traditional approaches, such as levelized-cost analysis, have limited applicability since they neglect grid interactions, such as the time-varying value of electricity. Therefore, this work developed DISPATCHES, a collection of novel multiscale simulation and optimization approaches to include the impact of grid interaction during the design of IES. The novel capabilities help stakeholders make market-informed decisions related to new investments in IES for a given electricity market. In addition, they help process designers avoid over-design/under-design components of an IES.

Traditionally, energy systems are designed in isolation by treating the electric grid as an infinite sink/source of power. An implicit assumption in this approach is that the operation of the system is not affected by the grid, and vice versa. This approach works well for systems that operate at baseload throughout. As the percentage of VRE increases in the generation mix, even generators that were designed to operate at baseload will need to ramp frequently to balance the variable power output from intermittent renewables. Consequently, the operation of the IES will be governed by the grid conditions, rendering the traditional approach detached from reality. A more sophisticated approach that is increasingly being used in the recent literature is the *price-taker approach*. Here, it is assumed that the operation of the IES is governed by the grid conditions, but the IES does not impact grid behavior. However, depending on the capacity of the system relative to the capacity of the node/bus, the IES can significantly impact the electricity prices at the node where it is located. The change in prices affects the revenue the IES receives, which in turn affects the optimal design of the IES. This report demonstrates that the predictions obtained with the price-taker approach deviate from the true solution and motivate the need to include market interactions during the design of the IES.

To address this need, we develop two new capabilities to go beyond price-taker: (1) modeling market interactions via machine learning-based surrogate models and embedding them in a conceptual design problem, and (2) a multiscale market simulation that integrates detailed process

models and abstract grid models for analyzing the performance of IES in an electric grid. These capabilities are described in detail in Chapters 2 and 3, respectively, of this report. Although the report demonstrates the capabilities with specific examples, they are generalizable and can be used for a wide variety of applications including designing flexible carbon capture systems, power and hydrogen co-production using solid oxide fuel cells/electrolyzers, etc.

Chapter 2 demonstrates the conceptual design using market surrogates for designing power and hydrogen co-production systems. In particular, we consider retrofitting an existing nuclear generator and an existing wind farm with a polymer electrolyte membrane-based electrolyzer for hydrogen production. The electrolyzer improves the flexibility of the nuclear generator to respond to grid conditions and helps the wind generator to beneficially use the curtailed power. In this case, both the electricity and hydrogen markets are tightly coupled, and the coupling governs the amount of power dispatched to the grid and the amount of power used for hydrogen production. Here, we demonstrate that the price-taker approach leads to an incorrect conclusion and a sub-optimal design in some cases. More specifically, in the nuclear study, there exists a break-even price of hydrogen for a given electricity market above which participating in the hydrogen market is profitable. We show that, for the assumed conditions, the price-taker variant that is commonly used in the literature overestimates the break-even hydrogen price by 28.5%. As a result, there is a range of selling prices of hydrogen for which the price-taker approach yields a sub-optimal design of the electrolyzer. Next, in the renewables (wind) case study, hybridizing a wind farm with an electrolyzer can increase the total revenue more than threefold under the assumed conditions. Here, we show that the optimal size of the electrolyzer obtained with the market surrogates approach is closer to the true optimum, which is obtained with extensive market simulations. We also show that the price-taker approach overestimates the net present value by 180%, and the market surrogates approach yields a better estimate, which overestimates the net present value by only 72%. Both case studies clearly demonstrate that the estimates obtained with the market surrogates approach are more accurate than those obtained with the price-taker approach. The methodology developed in this work can be easily adapted to other generators such as large natural gas-fired power plants, solar photovoltaics, biomass gasification, etc., which are retrofitted with an electrolyzer for hydrogen production.

Chapter 3 demonstrates the multiscale optimization capability for designing and analyzing a wind farm equipped with a large-scale energy storage device, e.g., battery. We consider retrofitting an existing wind farm with a battery storage system. The battery storage system can store curtailed power during periods with a low market price and discharge it to the grid when prices are high, acting to arbitrage in the energy market. In the multiscale optimization, we use a stochastic approach (see Section 3.2.3) to bid the wind-battery IES into the energy market by solving a stochastic optimization problem that maximizes the expected profit of the IES. We quantify the difference between designing a wind-battery IES using price-taker and the multiscale approach. The price-taker overestimates the IES economic value by more than 50% and ignores the IES/grid interaction. However, the multiscale approach shows that such interaction may increase the average market real-time electricity price up to 3.8$/MWh and reduce the IES renewable curtailment by up to 0.38MWh.

Contents

Chapter 1

Introduction

An integrated energy systems (IES) provides flexibility to generate, distribute, and consume energy by exploring synergies among various energy resources and technologies [1, 2]. IESs take multiple inputs such as renewable generators, batteries, and polymer electrolyte membrane (PEM) electrolyzers [3] and provide multiple products and services — energy storage [4, 5], cooling [6, 4, 7, 8], heating [6, 4, 7, 8, 9], and chemicals such as hydrogen [10, 5]. IESs that can flexibly supply clean electricity and hydrogen may prove valuable due to their ability to arbitrage across energy products. By combining them with different technologies, IESs increase efficiency and reduce carbon emissions during electricity production [11]. However, several challenges, such as decision-making under uncertainty and grid integration, are associated with the design, operation, and control decisions of the IES.

The state-of-the-art approach to handling the challenges in an IES is design and operation co-optimization, where IESs are modeled by laws of physics to optimize their economic performance such as with net present value (NPV). The price-taker approximation is widely used in energy system optimization problems, as highlighted in Table 1.1. Price-taker takes historical locational marginal prices (LMP) or forecast signals from independent system operators (ISO) and embeds them in the optimization problem to calculate electricity revenue and economic performance. Price-taker assumes that the (1) individual energy resource is insignificant to the entire power system capacity and therefore cannot affect market prices [12], (2) energy market can accept all electricity from an IES, and (3) IES does not impact the dispatch profile of other generators.

However, the growing consensus is that the price-taker assumption for IES optimization neglects key interactions with the electric grid, often resulting in misleading analyses. Emmanuel et al. [19] proposed a feedback price-taker approach to simulate the impact of increased storage deployment on energy prices and the resulting impact on revenue. Martinek et al. [20] compared the price-taker model and production cost models (PCM) and indicated that the price-taker model over-aggressively responds to small-magnitude or short-duration peaks in LMP. Frew et al. [21] optimized a nuclear power plant with hydrogen production systems and demonstrated that the traditional price-taker model could overestimate the value of the IES. This awareness of the flaws in the price-taker approach underscores the growing need for new approaches that consider the IES/market interaction in the optimization model.

The DISPATCHES project developed multiple workflows for analyzing integrated (hybrid) en-

Reference	**Technology**	**Participating Markets**	**Location**	**Key Findings**
Gomes et al. [13]	Wind + PV	DA Market	Iberian	Coordination of wind and photovoltaic systems can reduce energy deviations and trading risk.
Li et al. [14]	PV + Battery	RT Market	Japan	Greater inter-annual volatility of real-time spot prices adds more opportunity value to energy storage dispatch.
Wang et al. [15]	Wind + PV	DA Market / RT Market	PJM	The proposed energy management framework reduces the operation cost of IES.
Shao et al. [16]	Wind + Fossil + CHP	DA Market	Norway	The integration of heat and electricity systems provides multiple options to customers for fulfilling their energy demand.
Diaz et al. [17]	Hydro	DA Market	Spain	The hydroelectric generating unit characteristics are modeled in detail in order to obtain a good approximation.
Kang et al. [18]	Wind + Fossil	DA Market	CAISO	The fossil-renewable-CO_2-capture energy system provides considerable operational flexibility.

Table 1.1: Recent examples which used the price-taker approach for optimization of IES. Here, DA, RT, PV, and, CHP stand for day-ahead, real-time, photovoltaics, and combined heat power, respectively.

ergy systems in a larger electricity market context. All workflows can be broadly classified into two categories: *price-taker* and *market interaction* (see Figure 1.1). The price-taker approach uses LMPs from different electricity markets (day-ahead, real-time, etc.) as representative of the grid behavior in the respective markets. If the electricity price is low at a particular hour, then it implicitly assumes that there is a surplus production of electricity in the grid, so the generator should not dispatch power to the grid. In contrast, if the electricity price is high at a particular hour, then there is a high demand for electricity, so the generator can dispatch power to the grid. As shown in Figure 1.1, either historical LMP data from different Independent System Operators (ISO) or LMP data generated using a PCM can be used for the price-taker analysis. If desired, the uncertainty in the price signal can be accommodated by generating different statistically-similar realizations of the price signal using RAVEN and formulating a stochastic program.

Market interaction workflows are novel capabilities developed under DISPATCHES, and they include complex grid interactions in the conceptual design of integrated/hybrid energy systems. Here, we have two different workflows: (1) a multi-scale "double loop" market simulation that uses market-informed dynamic bid curves for optimal dispatch, and (2) formulate a conceptual design problem by embedding market interactions via data-driven surrogate models. The first and

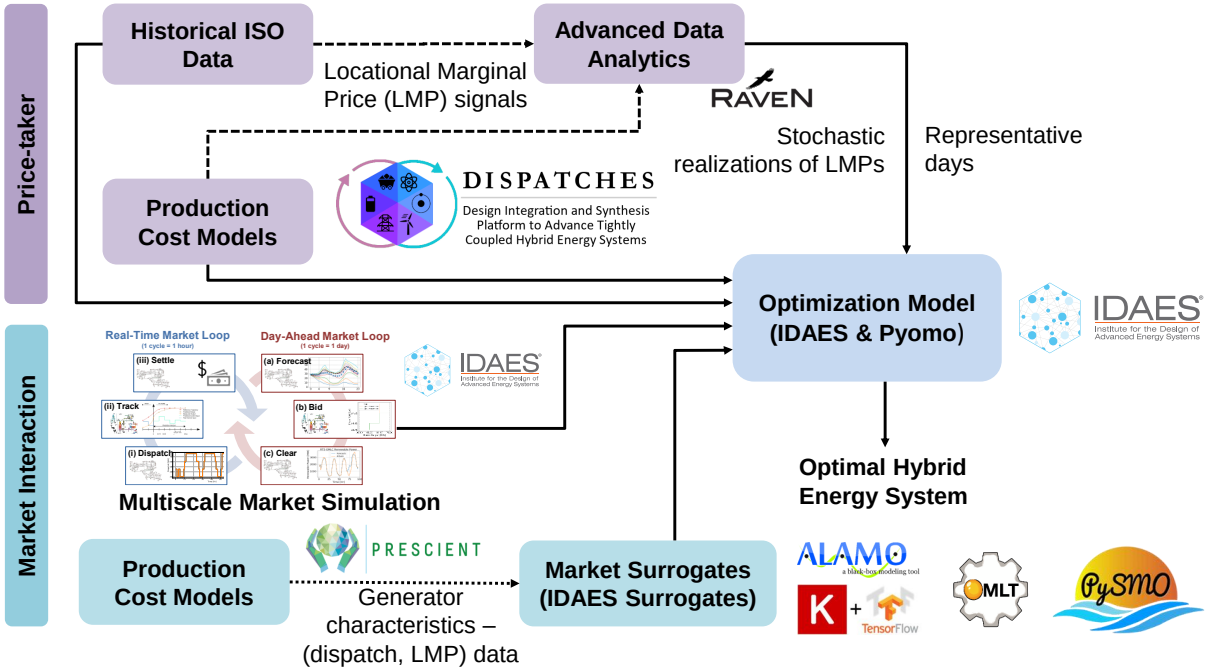

Figure 1.1: Workflows implemented in DISPATCHES can be broadly classified into two categories: *price-taker* and *market interaction*. The price-taker workflows (purple-coloured blocks) design IES using price data (either historical or data generated using a production cost model) and neglect any changes to the prices caused by the IES. If desired, uncertainty in the price data can be taken into account by generating multiple statistically similar price signals using RAVEN [22] and including them in the optimization model. The market interaction workflows (teal-colored blocks) account for the changes in the market behavior during the design of IES. All workflows leverage multiple U.S. Department of Energy-funded open-source platforms, including IDAES® [23], RAVEN [22], Prescient [24], Pyomo [25], etc.

second workflows will be elaborated in more detail in Chapter 3 and Section 2.3.3, respectively.

In this report, we propose a conceptual design with the surrogate model approach to quantify interactions between the IES and the electricity market. Surrogate models are trained from PCM simulations of different designs and accurately predict the electricity revenue and frequency of different dispatch scenarios according to given design variables.

The report is organized as follows: in Chapter 2, we consider the retrofit of a nuclear power plant and a renewable wind power plant with PEM electrolyzers to form IESs. We analyze and compare the results of the design and operation co-optimization of IESs using surrogate-assisted conceptual design optimization and price-taker optimization. Chapter 3 compares the price-taker optimization and multiscale optimization of a wind-battery IES with different battery sizes and capacities. Chapter 4 summarizes the methods and results from Chapters 2 and 3.

Chapter 2

Market-Informed Design of Electricity and Hydrogen Co-Production Systems

2.1 Introduction

Clean, carbon-free power generation technologies such as nuclear, wind, and solar photovoltaic are crucial for meeting the ambitious goal of decarbonizing the power sector by 2035. However, volatile grid conditions caused by the increasing penetration of intermittent renewables and several operational constraints can negatively affect both their profitability and grid operation, e.g., reliability. For example, although the marginal cost of production is zero for renewable generators such as wind farms, non-dispatchability due to uncertainty in energy production makes it challenging to realize the value of that cheap, carbon-free energy. Due to the variability of wind, the forecast of wind resources is a necessary input to grid scheduling, and errors in the forecast will require real-time operational adjustment. On the other hand, saturation of the energy market can lead to curtailment of renewables and low locational marginal prices (LMP), which result in inadequate revenues. Similarly, nuclear generators are prohibited from ramping due to safety regulations and must operate at baseload throughout. This reduces the flexibility of nuclear generators to respond to grid conditions, which may prefer all thermal generators (including nuclear generators) to undergo frequent ramping to balance the power output from variable renewable generators. Moreover, the increased price volatility caused by low-cost intermittent renewable generators could reduce the profitability of baseload nuclear generators.

One approach to increase the profitability of these systems is to participate in multiple markets to exploit the variability in electricity prices. A promising alternate market for these systems is the hydrogen market. When the electricity market is saturated, (i) renewable generators can beneficially use the curtailed power to produce hydrogen, and (ii) nuclear generators can "ramp down" by diverting power from the electricity market to produce hydrogen. The additional revenue from the hydrogen market can increase the overall profitability. Further, the added flexibility to "ramp" nuclear generators will increase their ability to dynamically respond to grid conditions. Hydrogen has several existing industrial applications and is expected to play a significant role in a future decarbonized economy. Hydrogen required for many industrial processes, such as ammonia synthesis and iron and steel manufacturing, is currently produced from natural gas. Production of hydro-

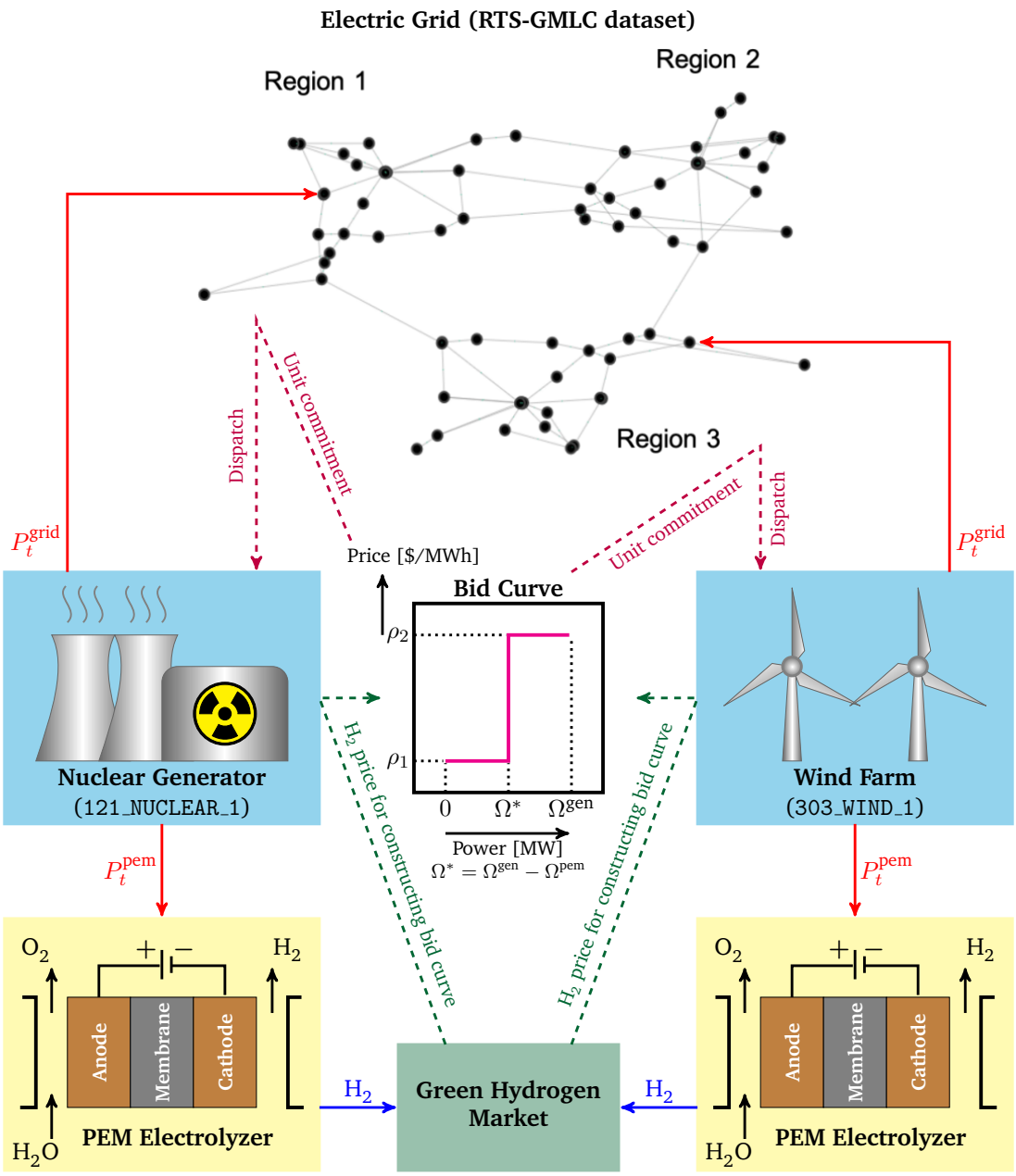

Figure 2.1: Hybridization of existing nuclear generator and wind farm with a low temperature electrolysis unit couples both electricity and hydrogen markets. In the electric grid, filled black circles denote nodes/buses and the gray arcs denote transmission lines. Bid curve denotes the offer price of electricity. Generator offers $[0, \Omega^{gen} - \Omega^{pem}]$ at price ρ_1 (in \$/MWh), and $[\Omega^{gen} - \Omega^{pem}, \Omega^{gen}]$ at price ρ_2, where Ω^{gen} and Ω^{pem} denote the capacities of the generator and electrolyzer, respectively. The price ρ_1 is typically chosen to be the marginal cost of the generator, and the price ρ_2 depends on the selling price of hydrogen. The bid curve is used by the grid operator to clear the market and determine the optimal dispatch of all the generators in the grid and the locational marginal prices.

gen using electricity from nuclear and renewable generators helps decarbonize those industries as well. Moreover, the produced hydrogen can be stored and used for peakers or can be blended with natural gas to reduce carbon emissions associated with its use. For these reasons, hybridizing renewable and nuclear generators to co-produce power and hydrogen is beneficial from operational, economic, and environment standpoints.

In this chapter, we analyze the overall economics of hybridizing an existing nuclear generator and a wind farm with a hydrogen production system for a given electricity market. In particular, we use a polymer electrolyte membrane-based (PEM) electrolyzer for low-temperature electrolysis (see Figure 2.1). Although the chosen technology is less efficient compared to high-temperature steam electrolysis, it has a higher technology readiness level (TRL) making it attractive for immediate deployment. Including market interactions while designing power and hydrogen co-production systems is important for two reasons:

1. At any point in time, the decision to participate in the electricity market vs. hydrogen market depends on the revenue generated from these markets per unit energy. This determines the optimal capacity factor of the electrolyzer such that the combined revenue from both markets is maximized.
2. Generators can actively participate in the hydrogen market by tailoring their price bid to the electricity market based on the selling price of hydrogen (see Figure 2.1). The modified price bid can substantially change the LMPs and dispatch of other generators in the grid depending on the size of the electrolyzer and the size of the generator with respect to the capacity of the node. The change in LMPs affects the revenue streams from each market, which in turn affects the design decisions (optimal size of the electrolyzer).

The novel capabilities developed under DISPATCHES (see Figure 1.1) account for the these two factors during the conceptual design.

The remainder of the chapter is organized as follows. Section 2.2 defines the problem statement. Section 2.3 describes the overall methodology and generalized mathematical formulations for optimizing co-production systems. Sections 2.4 and 2.5 present two case studies focusing on nuclear and wind generators, respectively. Finally, we present a few concluding remarks in Section 2.6.

2.2 Problem Statement

Given an existing generator participating in an electricity market, determine whether hybridizing it with a low-temperature electrolysis system for hydrogen production has favorable economic metrics, such as positive net present value (NPV). If yes, then determine the optimal size of the electrolyzer that maximizes the chosen economic metric. If not, then determine the selling price of hydrogen above which the hybridization is economically favorable. Finally, determine how the hybridized system impacts grid behavior; in particular, for hourly LMPs in both day-ahead and real-time markets.

Since the hydrogen market is in a nascent stage, the availability of data pertaining to demand and prices is limited. Therefore, we make two assumptions.

Assumption 1. Hydrogen price is time-invariant.

Assumption 2. There is no demand constraint for hydrogen. Therefore, all the hydrogen produced by the electrolyzer can be sold to the hydrogen market at any time. Conversely, if the hydrogen market is deemed non-profitable, then the generator can choose not to produce hydrogen at all.

2.3 Methods

We use the classical *price-taker* approach and the proposed *market surrogates* approach for designing co-production systems in the context of a grid. For illustration, we consider the **RTS-GMLC** dataset as the electric grid. RTS-GMLC is a synthetic grid that is representative of the southwest U.S. as described in [26] and available at `https://github.com/GridMod/RTS-GMLC`. It has 73 thermal generators, 81 renewable generators (wind, hydro, utility-scale photo-voltaic, and rooftop photo-voltaic), 73 buses, and 120 transmission lines. In particular, the grid has one nuclear generator. We simulate the grid using open-source production cost model (PCM) Prescient [24], available at `https://github.com/grid-parity-exchange/Prescient`. We consider the nuclear generator `121_NUCLEAR_1` located at the bus "Attlee" and the wind farm `303_WIND_1` located at the bus "Caesar" for hybridization with a PEM electrolyzer.

Hereafter, we refer to the parameters that govern the operation and dispatch of a generator, such as ramp rate, minimum uptime/downtime, maximum dispatchable capacity, bid curve, etc., as *generator characteristics*. The generator that is hybridized with an electrolyzer is referred to as *hybridized generator*.

The price-taker approach has two necessary steps and an optional third step (detailed description follows in Section 2.3.2):

PT1. Perform the *Base Case* PCM simulation to generate the day-ahead (DA) and real-time (RT) hourly LMPs at the node where the generator is located.

PT2. Formulate and solve the price-taker problem.

PT3. (Optional) Perform an annual PCM simulation with the generator characteristics fixed to the optimal solution obtained in **PT2** and compare the total revenue with that obtained in **PT2**. If the difference is substantial, then repeat **PT2** and **PT3** with the new DA and RT LMPs obtained in the PCM simulation. The intent is to reduce the difference over a few iterations, but there is no guarantee that it will converge.

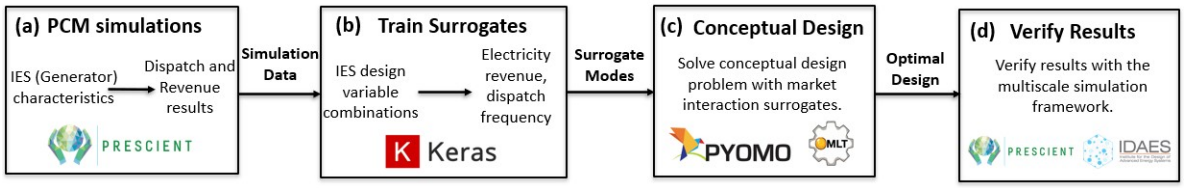

Figure 2.2: Conceptual design with market interaction surrogate models. In block (a), we extract data from PCM simulations of different IES (generator) characteristics. In block (b), we train surrogate models using the data from (a). We embed trained surrogate models in the optimization problem using `OMLT` [27] in block (c) and solve for the optimal IES design. In block (d), we use the multiscale simulation framework [1] to verify the optimal design from (c).

The market surrogates approach has three necessary steps and an optional fourth step (see Figure 2.2; a detailed description follows in Section 2.3.3):

MS1. Perform a *Characteristic Parameter Sensitivity Analysis* to generate optimal dispatch and LMP data for different generator characteristics of the hybridized generator.

MS2. Train a neural network-based surrogate model to predict the total annual revenue (function of DA and RT LMPs) and the dispatch as a function of generator characteristics.

MS3. Formulate and solve the conceptual design problem by embedding the surrogate models trained in **MS2**.

MS4. (Optional) Perform an annual PCM simulation with the generator characteristics fixed to the optimal design obtained in **MS3** and compare the total revenue with that obtained in **MS3**. If there is a significant difference in the results, then add the new generator characteristics and the corresponding optimal dispatch and revenue data to the training dataset and repeat **MS2** and **MS3**. Unlike the price-taker approach, this approach will eventually converge provided that the surrogate model accurately represents the data.

2.3.1 Parameter Settings for PCM Simulations

The PCM simulations for a grid containing the hybridized system are carried out by suitably modifying the generator characteristics of the hybridized generator, such as ramp rates, bid curve, etc. The parameters for the remaining generators in the grid are left at their default values listed in the RTS-GMLC dataset. Each PCM/Prescient simulation is run for all 366 days in year 2020 available in the RTS-GMLC dataset, with a 36-hour day-ahead unit commitment problem utilizing the forecast data for load and renewable units, and a 1-hour economic dispatch with no look-ahead and the real-time data for load and renewables production. All 120 transmission constraints are enforced for each unit commitment and economic dispatch problem. Each unit commitment problem is solved either with the FICO Xpress Solver [28] to a 1% optimality gap, or after exploring 1000 nodes in the branch-and-bound tree. Day-ahead energy prices are calculated utilizing the "approximated" convex hull price [29, 30], and real-time energy prices are calculated utilizing the standard locational marginal price. Slack variables are placed on the transmission limit constraints and at reference-bus power-balance constraints. In both the day-ahead and real-time pricing problem, the

value of violation for both types of slack variables is determined by a *shortfall price*. The shortfall price is the price at which the system either experiences a shortfall or an over-generation event. Prescient models the uncertainty inherent in day-ahead unit commitment, so when the economic dispatch problem is run, shortfall or over-generation can occur due to a mis-forecasting of load or renewables availability. For the simulations in this work, we choose a shortfall price well below the acknowledged value of lost load, because Prescient does not explicitly model all the recourse actions actually available to transmission system operators, such as intra-day commitments or manual operator interventions. Hence the shortfall price can also be thought of as the cost of these more expensive recourse actions to manage uncertainty in near real-time. Lastly, the *reserve* quantity is determined as a fraction of total load at each time step.

It is important that the renewables case describe how the generator characteristics differ between different approaches. The set of generator characteristics depends on the generator's type, and renewable and thermal generators have different characteristics. The original wind plant in the RTS-GMLC is a renewable generator, and in the PCM enumeration, the hybrid plant is modeled as two separate plants: the original renewable-type generator and a PEM virtual-type plant. However, the validation of the optimal renewable designs used the market integrated simulation workflow in [1], which changes the generator type to thermal. The renewable and virtual type plants do not provide reserves while thermal types participate in some reserve markets. Because the PCM enumeration plants were represented differently within the PCM, the revenue results are different for the PCM Enumeration vs. the validation of PCM enumeration. There are differences in dispatch and revenue due to each plant type's different properties and in the unit commitment solutions, which will have path-dependent effects down the entire year of results. RTS-GMLC (and unit commitment problems in general) can have thousands of near-optimal commitments within the 1% optimality tolerance utilized in the simulation. Different near-optimal solutions can cause significant differences in revenue among generators and different price spikes in the Real-Time Market due to uncertainty in renewable generation and load between day-ahead and real-time. Because of these factors, we can observe an average of a 10% difference in revenue for a single generator while achieving very similar system-level production costs [31].

2.3.2 Price-taker Approach

PT1. Base Case PCM Simulation

We generate the DA and RT LMP signals needed to solve the price-taker problem by performing a *base case* PCM simulation with the RTS-GMLC dataset. In the base case, the nuclear generator `121_NUCLEAR_1` is not hybridized, so it bids into the electricity market as a baseload generator at a marginal price of \$0/MWh. Similarly, the wind generator `303_WIND_1` is also not hybridized, so it dispatches the required power to the grid, and the excess power is curtailed. All grid-level parameters (such as wind resource, demand, etc.) are left at their default RTS-GMLC values, except the reserve quantity and the "shortfall" price. We choose the reserve (β^{res}) quantity to be 15%, a "shortfall" price ($\beta^{\text{shortfall}}$) of \$500/MWh for the nuclear case study, and \$1000/MWh for the renewables case study. Simulating both DA and RT markets using Prescient yields the locational marginal prices (LMPs) at all nodes. Later, in Section 2.4.3, we show that the price distribution changes when a generator is hybridized with an electrolyzer, thereby demonstrating the need to include market interactions when designing integrated energy systems.

Symbol	Definition
	List of Parameters
ψ^{pem}	Amount of hydrogen produced per unit energy [kg H_2/MWh]
ρ^{H_2}	Selling price of hydrogen [\$/kg H_2]
ρ_t^{LMP}	Locational marginal price of electricity at time t [\$/MWh]
ϕ_1^{gen}	Fixed O&M cost of the generator [\$/yr]
ϕ_1^{pem}	Fixed O&M cost of the PEM electrolyzer [\$/yr]
ϕ_2^{gen}	Variable O&M cost of the generator [\$/MWh]
ϕ_2^{pem}	Variable O&M cost of the PEM electrolyzer [\$/MWh]
γ^{pem}	Overnight capital cost of the PEM electrolyzer [\$/MW]
λ	Lifetime of the plant [yr]
τ	Corporate tax rate [-]
δ	Discount rate [-]
ξ	Annualization factor, $\xi = (1-(1+\delta)^{-\lambda})/\delta$
μ	Number of hours in a year ($\mu = 8784$ for this work)
β^{res}	Reserves as a percentage of total load
$\beta^{\text{shortfall}}$	"Shortfall" price
	List of Variables
Ω^{gen}	Design capacity of the generator [MW]
Ω^{pem}	Design capacity of the electrolyzer [MW]
P_t^{gen}	Power produced by the generator at time t [MW]
P_t^{grid}	Power sold to the grid at time t [MW]
P_t^{pem}	Power input to the electrolyzer at time t [MW]
$HREV$	Annual revenue from the sale of H_2 [\$/yr]
$EREV$	Annual revenue from the sale of electricity to grid [\$/yr]
FOM	Total annual fixed O&M cost [\$/yr]
VOM	Total annual variable O&M cost [\$/yr]
$CAPEX$	Total overnight capital cost [\$]
DEP	Annual depreciation [\$/yr]
TAX	Annual corporate tax [\$/yr]
$PROFIT$	Annual net profit [\$/yr]
NPV	Annualized net present value [\$/yr]

Table 2.1: Definition of parameters and variables

PT2. Price-taker Formulation

The *price-taker formulation* for retrofitting an existing generator with a PEM electrolyzer-based hydrogen production system is given below.

$$\max \quad NPV \tag{2.1a}$$
$$\text{s.t.} \quad P_t^{\text{gen}} = f^{\text{gen}}(\Omega^{\text{gen}}, \dots), \quad \forall\, t \in \mathcal{T} \tag{2.1b}$$
$$P_t^{\text{gen}} = P_t^{\text{grid}} + P_t^{\text{pem}}, \quad \forall\, t \in \mathcal{T} \tag{2.1c}$$
$$0 \leq P_t^{\text{pem}} \leq \Omega^{\text{pem}}, \quad \forall\, t \in \mathcal{T} \tag{2.1d}$$
$$HREV = \sum_{t \in \mathcal{T}} \psi^{\text{pem}} \cdot P_t^{\text{pem}} \cdot \rho^{\text{H}_2} \tag{2.1e}$$
$$EREV = \sum_{t \in \mathcal{T}} \rho_t^{\text{LMP}} \cdot P_t^{\text{grid}} \tag{2.1f}$$
$$FOM = \phi_1^{\text{gen}} \cdot \Omega^{\text{gen}} + \phi_1^{\text{pem}} \cdot \Omega^{\text{pem}} \tag{2.1g}$$
$$VOM = \sum_{t \in \mathcal{T}} \left(\phi_2^{\text{gen}} \cdot P_t^{\text{gen}} + \phi_2^{\text{pem}} \cdot P_t^{\text{pem}}\right) \tag{2.1h}$$
$$CAPEX = \gamma^{\text{pem}} \cdot \Omega^{\text{pem}} \tag{2.1i}$$
$$DEP = CAPEX/\lambda \tag{2.1j}$$
$$TAX \geq 0 \tag{2.1k}$$
$$TAX \geq \tau \cdot (EREV + HREV - FOM - VOM - DEP) \tag{2.1l}$$
$$PROFIT = EREV + HREV - FOM - VOM - TAX \tag{2.1m}$$
$$NPV = PROFIT - (1/\xi) CAPEX \tag{2.1n}$$

Here, $\mathcal{T} = \{1, 2, \dots, \mu\}$ denotes the set of hours in a year. We use lower case Greek letters for parameters (e.g., ψ^{pem}, ϕ_1^{gen}), upper case Greek letters for design/capacity variables (e.g., Ω^{gen}, Ω^{pem}), and italicized upper case letters (e.g., P_t^{grid}, P_t^{gen}) and text (e.g., $CAPEX$, FOM) for operational variables and cash flow expressions, respectively. The definitions of variables and parameters used in the above formulation can be found in Table 2.1. The parameters and variables with superscripts gen and pem correspond to the generator and electrolyzer, respectively.

Objective (2.1a) maximizes the annualized NPV. Constraint (2.1b) computes the power produced by the generator at time t as a function of the generator capacity (Ω^{gen}), and other parameters (such as wind/solar resource for wind/photovoltaic farms), etc. Constraint (2.1c) models the power balance at time t, i.e., the power output from the generator (P_t^{gen}) must be equal to the sum of power sold to the grid (P_t^{grid}) and power input to the electrolyzer (P_t^{pem}). Constraint (2.1d) ensures that the power input to the electrolyzer at time t does not exceed the capacity of the electrolyzer (Ω^{pem}). Constraint (2.1e) computes the revenue from the hydrogen market as the sum of revenues from hydrogen production over the entire time horizon. Constraint (2.1f) computes the revenue from the electricity market. Constraints (2.1g) and (2.1h) compute the annual fixed operation and maintenance (O&M) and variable O&M costs for the entire retrofitted system, respectively. Constraint (2.1i) computes the overnight capital expenditure for installing the electrolyzer. The capital cost of the generator is not included because we are considering a retrofit of an existing generator. Constraint (2.1j) computes the annual depreciation value assuming a straight line depreciation with zero salvage value. Constraints (2.1k) and (2.1l) compute the corporate tax. If the system is not profitable i.e., $EREV + HREV - FOM - VOM - DEP \leq 0$, then (2.1k) ensures that the corporate tax is zero. Since a higher corporate tax reduces the annualized NPV, either the

constraint (2.1k) or the constraint (2.1l) would be binding for the optimal solution as required. Finally, constraints (2.1m) and (2.1n) compute the net profit and the annualized NPV, respectively. The optimization problem has one design decision[1] (Ω^{pem}) and $3 \cdot \mu$ operating decisions (P_t^{gen}, P_t^{grid}, and P_t^{pem}). If the function f^{gen} is linear, then the optimization formulation becomes a linear program, and it can be solved efficiently with Gurobi [32], CPLEX, XPRESS, CBC, GLPK, or other optimization solvers. This generalized formulation can be used for both nuclear and renewable generators by suitably modifying constraint (2.1b).

Generators typically participate in both DA and RT markets. Often, the locational marginal prices in both markets differ substantially, so it is not clear which price signal must be used for the analysis. Here, we present four variants, **V1** through **V4**, of the price-taker problem and compare the results obtained.

V1 Solve (2.1) with $\rho_t^{\text{LMP}} = \left(\rho_t^{\text{LMP}}\right)^{\text{DA}} \ \forall\, t \in \mathcal{T}$ in (2.1f), where $\left(\rho_t^{\text{LMP}}\right)^{\text{DA}}$ denotes the DA LMP.

V2 Solve (2.1) with $\rho_t^{\text{LMP}} = \left(\rho_t^{\text{LMP}}\right)^{\text{RT}} \ \forall\, t \in \mathcal{T}$ in (2.1f), where $\left(\rho_t^{\text{LMP}}\right)^{\text{RT}}$ denotes the RT LMP.

V3 Solve (2.1) with $\rho_t^{\text{LMP}} = \max\left\{\left(\rho_t^{\text{LMP}}\right)^{\text{DA}}, \left(\rho_t^{\text{LMP}}\right)^{\text{RT}}\right\} \ \forall\, t \in \mathcal{T}$ in (2.1f).

V4 This variant is a two-step method where (2.2) and (2.3) are solved sequentially. In (2.3), $\left(P_t^{\text{grid}}\right)^{\text{DA}}$ is a parameter and it denotes the optimal power output to the grid obtained in (2.2). The revenue and NPV values obtained in (2.3) are taken to be the optimal cash flows for the system.

$$\text{Step 1:} \quad \left\{ \begin{array}{ll} \max & NPV \\ \text{s.t.} & (2.1\text{b}) - (2.1\text{e}),\ (2.1\text{g}) - (2.1\text{n}) \\ & EREV = \sum_{t \in \mathcal{T}} \left(\rho_t^{\text{LMP}}\right)^{\text{DA}} \cdot P_t^{\text{grid}} \end{array} \right\} \tag{2.2}$$

$$\text{Step 2:} \quad \left\{ \begin{array}{ll} \max & NPV \\ \text{s.t.} & (2.1\text{b}) - (2.1\text{e}),\ (2.1\text{g}) - (2.1\text{n}) \\ & EREV = \sum_{t \in \mathcal{T}} \left(\rho_t^{\text{LMP}}\right)^{\text{DA}} \cdot \left(P_t^{\text{grid}}\right)^{\text{DA}} + \left(\rho_t^{\text{LMP}}\right)^{\text{RT}} \cdot \left(P_t^{\text{grid}} - \left(P_t^{\text{grid}}\right)^{\text{DA}}\right) \end{array} \right\} \tag{2.3}$$

Variants **V1**, **V2**, and **V3** allow simultaneous optimization of design (Ω^{pem}) and operational (P_t^{grid} and P_t^{pem}) decisions. Variant **V4** is a new contribution, and it is inspired by the order of market clearing. **V4** optimizes the operational decisions for a fixed design, so it requires enumeration over the entire design space. Thus, it is computationally more expensive than the first three variants. We illustrate that the results obtained with **V4** can be substantially different compared to those obtained with **V1**, **V2**, and **V3** with an example in Section 2.4.

[1] For a retrofit, the capacity of the generator (Ω^{gen}) is fixed, so it is not a decision variable.

2.3.3 Market Surrogates Approach

MS1. Perform Characteristic Parameter Sensitivity Analysis

Characteristic parameter sensitivity analysis refers to a set of PCM/Prescient simulations performed by hybridizing the generator of interest for different values of generator characteristics of the hybridized generator. We sample several points from the domain of generator characteristics. For each point in the sample, we fix the generator characteristics to the chosen point and perform an annual electricity market simulation using a PCM. Each PCM simulation solves unit commitment and economic dispatch problems in a rolling-horizon framework and yields DA and RT dispatch for all generators in the grid and LMPs at all nodes.

For example, the electrolyzer enables the hybridized nuclear generator to ramp between $[\Omega^{\text{npp}} - \Omega^{\text{pem}}, \Omega^{\text{npp}}]$, where Ω^{npp} and Ω^{pem} denote the capacity of the baseload nuclear generator and the maximum/design capacity of the electrolyzer, respectively. Further, the hybridized generator can account for the hydrogen market by changing its bid to the electricity market as shown in Figure 2.1. In particular, the hybridized generator now bids $[0,\ \Omega^{\text{npp}} - \Omega^{\text{pem}}]$ at \$0/MWh (ρ_1 in Figure 2.1) and $[\Omega^{\text{npp}} - \Omega^{\text{pem}}, \Omega^{\text{npp}}]$ at a higher price (see ρ_2 in Figure 2.1), which we refer to as the *electrolyzer indifference point*. The electrolyzer indifference point denotes the threshold price below which the hydrogen market generates more revenue per unit of energy and above which the electricity market generates more revenue per unit of energy. Thus, it is a function of the selling price of hydrogen, and it increases as the selling price of hydrogen increases. Therefore, in the nuclear case study, we vary two generator characteristics (ramp rate and bid curve) by varying Ω^{pem} and electrolyzer indifference point, and obtain the corresponding dispatch and LMP data. To have sufficient data for training a neural network, we perform the parameter sweep for the following values of reserve and shortfall price: (i) $\beta^{\text{res}} = 10\%$ and $\beta^{\text{shortfall}} = \$500$/MWh, (ii) $\beta^{\text{res}} = 10\%$ and $\beta^{\text{shortfall}} = \$1000$/MWh, and (iii) $\beta^{\text{res}} = 15\%$ and $\beta^{\text{shortfall}} = \$1000$/MWh, in addition to the base case value of $\beta^{\text{res}} = 15\%$ and $\beta^{\text{shortfall}} = \$500$/MWh. This also makes the model more flexible by allowing us to consider the impact of market settings. The characteristic parameter sensitivity analysis for the renewable case study is set up in an analogous manner.

MS2. Train surrogate models to predict market outcomes as a function of generator characteristics

Using the data obtained in **MS1**, we train a neural network-based surrogate model to predict the total revenue (output) the generator receives and its dispatch profile (output) as a function of the generator characteristics (inputs). Mathematically,

$$EREV = f^{\text{erev}}\left(\Omega^{\text{pem}},\ B,\ \beta^{\text{res}},\ \beta^{\text{shortfall}}\right) \tag{2.4}$$

where f^{erev} is the neural network model and B is the electrolyzer indifference point, respectively. In the training data, the total revenue is calculated as $\sum_{t\in\mathcal{T}}(\rho_t^{\text{LMP}})^{\text{DA}}\cdot(P_t^{\text{grid}})^{\text{DA}} + (\rho_t^{\text{LMP}})^{\text{RT}}\cdot((P_t^{\text{grid}})^{\text{RT}} - (P_t^{\text{grid}})^{\text{DA}})$, where P_t^{grid} and ρ_t^{LMP} denote the dispatch and LMP at time t , and the superscripts DA and RT denote that the values correspond to the DA and RT markets, respectively.

Unlike the total revenue, the dispatch data for each point in the training data is a time series,

$\{(P_t^{\text{gen}})^{\text{RT}}\}_{t\in\mathcal{T}}$, containing μ $(= 366 \times 24)$ elements. The amount of data generated in **MS1** is typically not sufficient to train a neural network that can accurately predict the high-dimensional dispatch profile. Therefore, we do the following instead. For convenience, we drop the superscript RT, but note that the values of all variables correspond to the real-time market.

1. Let $V_{t,p} = [\chi_{t,p}^{\text{gen}}, \chi_{t,p}^{\text{pem}}, \chi_{t,p}^{\text{grid}}]$, for every $t \in \mathcal{T}$ and $p \in \mathcal{D} := \{1, 2, \ldots, D\}$, the set of training data, where[2] $\chi_{t,p}^{\text{gen}} = P_{t,d}^{\text{gen}}/\Omega_p^{\text{gen}}$, $\chi_{t,p}^{\text{pem}} = P_{t,d}^{\text{pem}}/\Omega_p^{\text{gen}}$, and $\chi_{t,p}^{\text{grid}} = P_t^{\text{grid}}/\Omega_p^{\text{gen}}$. In terms of χ variables, the total power produced by the generator $P_{p,\text{ total}}^{\text{gen}} = \sum_{t\in\mathcal{T}} \chi_{t,p}^{\text{gen}} \cdot \Omega_p^{\text{gen}}$. The total power to the electrolyzer and to the grid in terms of χ variables can be obtained in a similar manner.

2. Cluster the data $\{V_{t,p}\}_{t\in\mathcal{T},\, p\in\mathcal{D}}$ into S clusters using the k-means clustering technique. Let $\mathcal{S} := \{1, 2, \ldots, S\}$ denote the set of clusters, $\widetilde{V}_s$ be the centroid of cluster s, and $\mathcal{T}_{p,s} = \{t \in \mathcal{T},\ \text{if } V_{t,p} \in \text{ cluster } s\}$, for every $p \in \mathcal{D}$ and $s \in \mathcal{S}$. Then, in terms of centroids of clusters, the total power can be obtained as

$$\begin{aligned} P_{p,\text{ total}}^{\text{gen}} &= \sum_{s\in\mathcal{S}} \text{card}(\mathcal{T}_{p,s}) \cdot \tilde{\chi}_s^{\text{gen}} \cdot \Omega_p^{\text{gen}} \\ &= \Omega_p^{\text{gen}} \cdot \text{card}(\mathcal{T}) \cdot \sum_{s\in\mathcal{S}} \frac{\text{card}(\mathcal{T}_{p,s})}{\text{card}(\mathcal{T})} \cdot \tilde{\chi}_s^{\text{gen}} \\ &= \mu \cdot \Omega_p^{\text{gen}} \cdot \sum_{s\in\mathcal{S}} F_{p,s} \cdot \tilde{\chi}_s^{\text{gen}} \end{aligned} \tag{2.5}$$

   Here, $\text{card}(\mathcal{T})$ denotes cardinality of set $\mathcal{T}$, $F_{p,s} = \text{card}(\mathcal{T}_{p,s})/\,\text{card}(\mathcal{T})$, and note that $\text{card}(\mathcal{T}) = \mu$. The total power to the electrolyzer and to the grid in terms of χ variables can be obtained in a similar manner.

3. Train a neural network with Ω^{pem}, B, β^{res}, and $\beta^{\text{shortfall}}$ as inputs and $F_1, F_2, \ldots, F_S$ described in Equation (2.5) as outputs. Mathematically,

$$F_s = f_s^{\text{disp}}\left(\Omega^{\text{pem}}, B, \beta^{\text{res}}, \beta^{\text{shortfall}}\right), \quad \forall\ s \in \mathcal{S} \tag{2.6}$$

   where f_s^{disp} denotes a neural network model. These surrogate models are used to determine the total power produced by a generator, the total power input to the electrolyzer, and the total power sold to the grid.

MS3. Solve the conceptual design optimization problem with embedded market surrogates.

We formulate a conceptual design problem using the surrogates constructed in **MS2**. The generalized formulation for conceptual design is given below:

$$\max \quad NPV \tag{2.7a}$$

$$\text{s.t.} \quad EREV = f^{\text{erev}}\left(\Omega^{\text{pem}}, B, \beta^{\text{res}}, \beta^{\text{shortfall}}\right) \tag{2.7b}$$

[2] For most generators, these variables are related; but they are independent for renewable generators because of curtailment.

$$F_s = f_s^{\text{disp}}\left(\Omega^{\text{pem}}, B, \beta^{\text{res}}, \beta^{\text{shortfall}}\right), \quad \forall\, s \in \mathcal{S} \tag{2.7c}$$

$$P_{\text{total}}^{\text{gen}} = \mu \cdot \Omega^{\text{gen}} \cdot \sum_{s\in\mathcal{S}} F_s \cdot \tilde{\chi}_s^{\text{gen}} \tag{2.7d}$$

$$P_{\text{total}}^{\text{grid}} = \mu \cdot \Omega^{\text{gen}} \cdot \sum_{s\in\mathcal{S}} F_s \cdot \tilde{\chi}_s^{\text{grid}} \tag{2.7e}$$

$$P_{\text{total}}^{\text{pem}} = \mu \cdot \Omega^{\text{gen}} \cdot \sum_{s\in\mathcal{S}} F_s \cdot \tilde{\chi}_s^{\text{pem}} \tag{2.7f}$$

$$HREV = \psi^{\text{pem}} \cdot P_{\text{total}}^{\text{pem}} \cdot \rho^{\text{H}_2} \tag{2.7g}$$

$$FOM = \phi_1^{\text{gen}} \cdot \Omega^{\text{gen}} + \phi_1^{\text{pem}} \cdot \Omega^{\text{pem}} \tag{2.7h}$$

$$VOM = \phi_2^{\text{gen}} \cdot P_{\text{total}}^{\text{gen}} + \phi_2^{\text{pem}} \cdot P_{\text{total}}^{\text{pem}} \tag{2.7i}$$

$$CAPEX = \gamma^{\text{pem}} \cdot \Omega^{\text{pem}} \tag{2.7j}$$

$$DEP = CAPEX/\lambda \tag{2.7k}$$

$$TAX \geq 0 \tag{2.7l}$$

$$TAX \geq \tau \cdot (EREV + HREV - FOM - VOM - DEP) \tag{2.7m}$$

$$PROFIT = EREV + HREV - FOM - VOM - TAX \tag{2.7n}$$

$$NPV = PROFIT - (1/\xi) \cdot CAPEX \tag{2.7o}$$

In this work, we use `OMLT` [27] to embed neural network surrogate models in the optimization model implemented in Pyomo [33]. The parameters and variables are defined in the same manner as in Table 2.1. Objective (2.7a) maximizes the NPV. Constraints (2.7b) – (2.7f) compute the revenue and the total power produced by the generator and total power input to the electrolyzer as described in **MS2**. The remaining cashflow calculations are the same as those in constraint (2.1g) – (2.1n).

For a baseload generator, construction of the surrogate model for the dispatch can be simplified. Instead of clustering the dispatch profile and training surrogate models for the weights (F_s) associated with each cluster, we train a surrogate model for the total fraction of power produced by the generator that is sold to the grid. Mathematically, we construct a surrogate model of the form

$$K^{\text{gen}} = f^{\text{disp}}\left(\Omega^{\text{pem}}, B, \beta^{\text{res}}, \beta^{\text{shortfall}}\right) \tag{2.8}$$

In terms of K^{gen}, the dispatch surrogate models in (2.7d), (2.7e), and (2.7f) can now be simplified to

$$P_{\text{total}}^{\text{gen}} = \mu \cdot \Omega^{\text{gen}} \tag{2.9a}$$

$$P_{\text{total}}^{\text{grid}} = \mu \cdot \Omega^{\text{gen}} \cdot K^{\text{gen}} \tag{2.9b}$$

$$P_{\text{total}}^{\text{pem}} = P_{\text{total}}^{\text{gen}} - P_{\text{total}}^{\text{grid}} \tag{2.9c}$$

Equation (2.9a) is valid because the generator produces baseload power throughout. Equation (2.9b) computes the total power sold to the grid in terms of K^{gen}. Finally, since there is no curtailment, the total power input to the electrolyzer must be equal to the difference between the total power produced and the total power sold to the grid via (2.9c). We also add

$$\Omega^{\text{gen}} \cdot \mu \cdot (1 - K^{\text{gen}}) \leq \Omega^{\text{pem}} \cdot \mu \tag{2.10}$$

The left hand side denotes the total energy input to the electrolyzer, and the right hand side denotes the maximum energy that the electrolyzer can consume in a year. In other words, the above

inequality ensures that the capacity factor of the electrolyzer is less than one. This constraint is needed because the surrogate model for K^{gen} is not exact. As a result, it sometimes takes a value that makes the capacity factor of the electrolyzer slightly greater than one. Adding the constraint to the model will prevent such solutions. We use (2.8), (2.9a) – (2.9c), and (2.10) for the nuclear case study and (2.7c) – (2.7f) for the renewable case study.

2.3.4 Computational Environment

Implementation of both the price-taker and market surrogates approaches requires several open-source and commercial software applications. Here, we list the software used to generate the results shown in this report. We use `IDAES v2.0.0` [23] and `Pyomo v6.5.0` [25] to formulate optimization models. The surrogate models for market interactions were trained using `TensorFlow-KERAS v2.9.1`, and they are embedded in the optimization model using `OMLT v1.1.0` [27]. Linear optimization models are solved using `Gurobi v10.0` [32], and nonlinear optimization models are solved using `IPOPT v3.13.2` [34]. Finally, the unit commitment and economic dispatch models in Prescient are solved using `FICO Xpress` [28].

2.4 Case Study: Retrofit a Nuclear Power Plant

In this case study, we consider retrofitting the nuclear generator `121_NUCLEAR_1` in the RTS-GMLC dataset with a PEM electrolyzer for hydrogen production (see Figure 2.1). Our goal is to determine the optimal size of the electrolyzer for a given electricity market that maximizes the net present value (NPV) of the entire hybridized system. Although participation in both markets can be attractive, the overall economics would be favorable only if the additional revenue obtained from the hydrogen market is high enough to recover the capital investment needed for the retrofit and other operational and maintenance costs. We perform the analysis with both the price-taker and market surrogates approaches and compare the results. We have also analyzed this problem with the traditional techno-economic analysis, and the results are presented in Appendix A.

Parameter	Definition	Value	Reference
ψ^{pem}	Amount of H_2 produced per unit energy [kg/MWh]	20	[35]
γ^{pem}	Overnight capital cost of the electrolyzer [$/MW]	1.2×10^6	[36][3]
ϕ_1^{npp}	Fixed O&M cost for the nuclear generator [$/MW-yr]	120,000	Assumption[4]
ϕ_1^{pem}	Fixed O&M cost for the electrolyzer [$/MW-yr]	$0.03 \times \gamma^{\text{pem}}$	Assumption[5]
ϕ_2^{npp}	Variable O&M cost for the nuclear generator [$/MWh]	2.3	Assumption[4]
ϕ_2^{pem}	Variable O&M cost for the electrolyzer [$/MWh]	0	Assumption
λ	Lifetime of the plant [yr]	30	Assumption
τ	Corporate tax rate [-]	20%	Assumption
δ	Discount rate [-]	8%	Assumption
ξ	Annualization factor: $(1-(1+\delta)^{-\lambda})/\delta$		
ω	Number of hours in a year	8784	
β^{res}	Reserves as percentage of total load [-]	15%	Assumption
$\beta^{\text{shortfall}}$	"Shortfall" price [$/MWh]	500	Assumption

Table 2.2: Parameter values used for the nuclear case study.

2.4.1 Results: Price-taker Approach

We run the base case PCM simulation as described in **PT1** (see Section 2.3.2) to obtain the DA and RT LMP data at the bus Attlee. Figure 2.3 shows the distribution of prices in both markets at this bus. Observe that the RT market has several price spikes (>$100/MWh) caused due to shortfall (see Section 2.3.1), and these price spikes are not present in the DA market. We use these price

[3]The capital cost of electrolyzers reported in [36] were in the range of $800/kW to $1500/kW. For this analysis, we chose a number that is close to the average of the limits.

[4]Assuming the capacity factor of the nuclear power plant to be 92.5% [37], the assumed fixed and variable O&M costs add up to $17.11/MWh. This cost is lower than the O&M costs for most nuclear power plants which is around $23.62/MWh [38]. Nevertheless, we use the lower estimate because the average electricity prices for the RTS-GMLC dataset are much lower than those for real electricity markets.

[5]Annual fixed O&M cost of the electrolyzer is assumed to be 3% of the capital cost. This is a reasonable assumption for most systems. The variable O&M cost of the electrolyzer is ignored here, since it tends to be small.

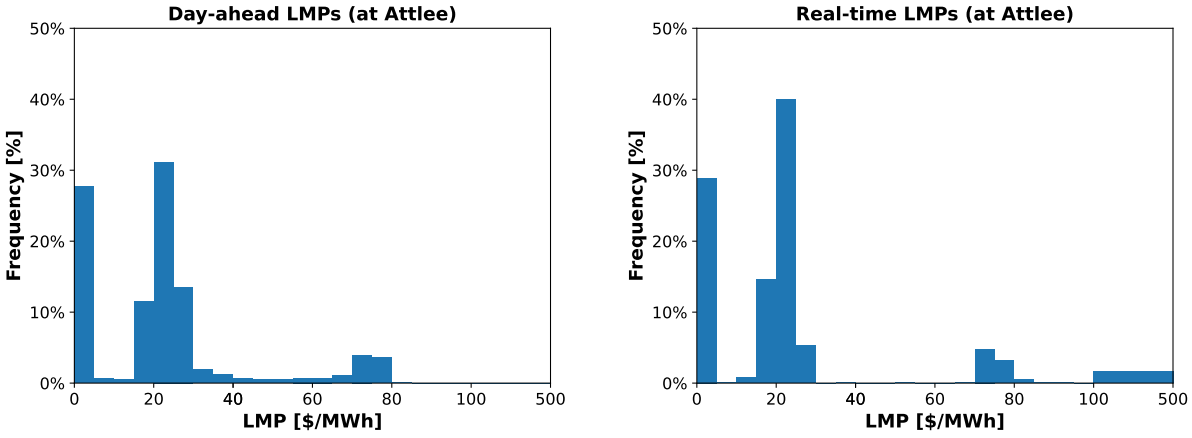

(a) (b)

Figure 2.3: Histograms of (a) DA and (b) RT LMPs at bus Attlee in the base case (i.e., baseload nuclear generator without an electrolyzer).

signals to formulate the price-taker problem.

Since the nuclear generator always operates at baseload, we solve the price-taker problem by modifying the constraint (2.1b) to $P_t^{\text{npp}} = \Omega^{\text{npp}} = 400, \forall\, t \in \mathcal{T}$, where $\Omega^{\text{npp}} = 400$ MW denotes the capacity of the nuclear generator `121_NUCLEAR_1`. The parameter values[3] can be found in Table 2.2. Using the price signals in Figure 2.3, we analyze the nuclear case study with all four price-taker variants (**V1** through **V4**). The results are shown in Figures 2.4 – 2.7.

Figure 2.4 compares the revenue from the electricity market obtained with all four variants. Observe that the overall trend obtained with the first three variants is similar, but the magnitude is very different. The magnitude of the revenue obtained with the RT price signal (**V2**) is higher than that obtained with the DA price signal (**V1**) because the former tends to have more price spikes compared to the latter (see Figure 2.3). Next, **V3** uses maximum of DA and RT prices, so the revenue in this case is higher than that obtained with both **V1** and **V2**. Finally, the revenue trend obtained with **V4**, i.e., the two-step method (see Figure 2.4(d)) is very different compared to the first three variants. In **V1**, **V2**, and **V3** the electricity revenue decreases with an increase in the ratio of capacities for all values of the selling price of hydrogen (see Figures 2.4(a), 2.4(b), and 2.4(c)). However, in **V4**, the revenue from the electricity market increases (respectively, decreases) with an increase in the ratio of capacities when the selling price of hydrogen is less (respectively, more) than $\sim$\$1.2/kg. We hypothesize that this is due to complex interactions between the DA and RT markets.

Figure 2.5 shows the revenue obtained from the hydrogen market with all four variants. The overall trend and magnitude obtained with all four variants are similar. Nevertheless, the revenue value obtained with **V3** is less than that obtained with **V1**, **V2**, and **V4**. This is because the electricity market is more profitable in **V3**, so the hybridized nuclear generator produces less hydrogen, which results in a lower revenue from the hydrogen market.

Figure 2.6 compares the annualized NPV obtained with all four variants. Although the magnitude differs, the overall trend obtained with the first two variants is similar (see Figures 2.6(a) and

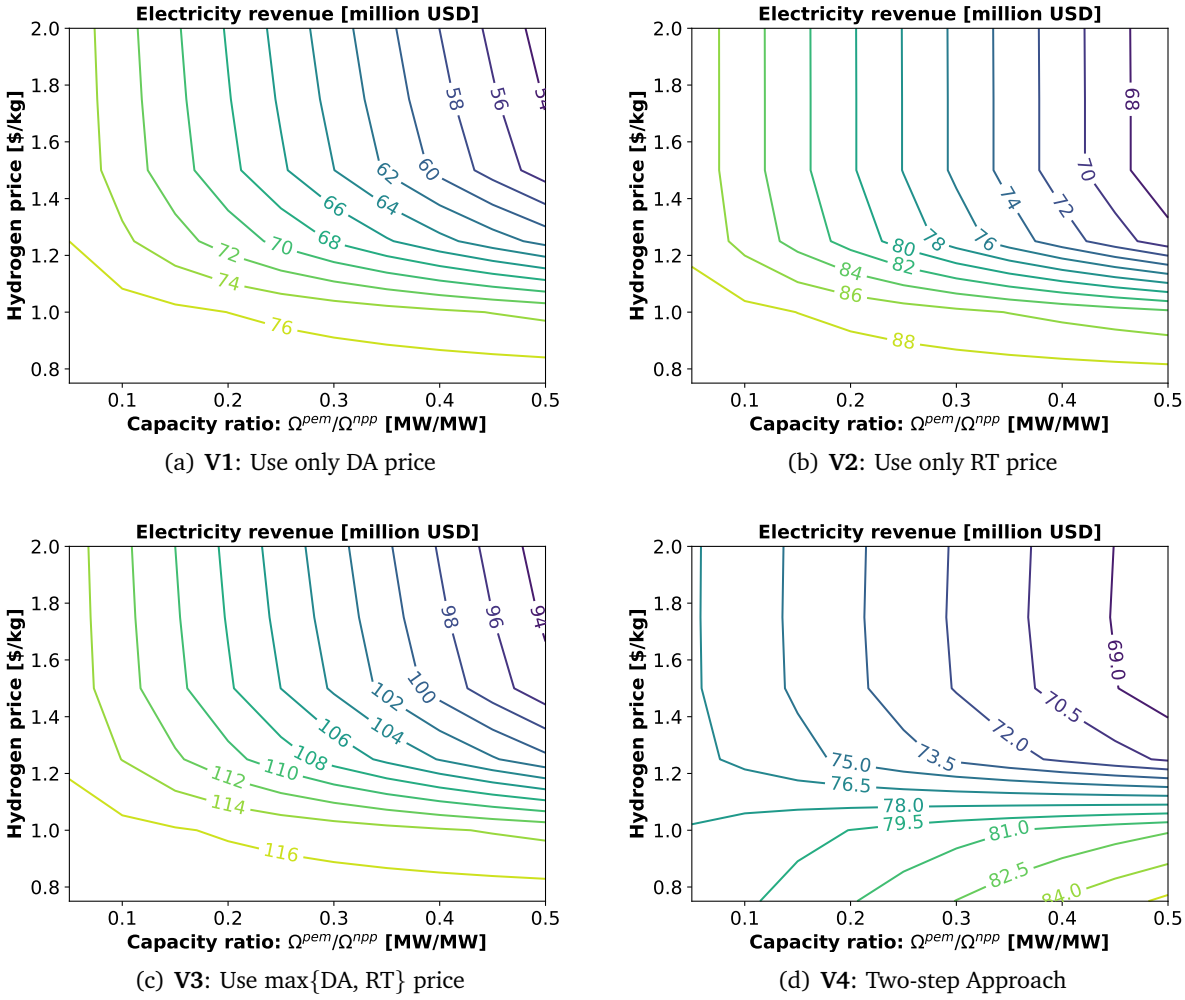

(a) **V1**: Use only DA price

(b) **V2**: Use only RT price

(c) **V3**: Use max{DA, RT} price

(d) **V4**: Two-step Approach

Figure 2.4: Electricity revenue predicted by different price-taker variants.

2.6(b)). We observe that there is a threshold selling price of hydrogen (∼$1.8/kg) above which the annualized NPV increases with an increase in the ratio of capacities. This implies that the revenue from the hydrogen market is not sufficient to recover the capital investment when the selling price of hydrogen is less than $1.8/kg, so an electrolyzer must not be built in this case. However, if the selling price of hydrogen is above $1.8/kg, then the revenue from the hydrogen market is high enough to recover the capital investment, so installing the biggest electrolyzer admissible maximizes the NPV. We draw a similar conclusion with **V4**, but the threshold selling price of hydrogen is lower, ∼$1.2/kg (see Figure 2.6(d)). In contrast, with **V3**, we observe that installing a PEM electrolyzer is not profitable provided that the selling price of hydrogen is lower than $2/kg.

Finally, Figure 2.7 compares the optimal capacity factor of the electrolyzer obtained with all four variants. The capacity factor increases monotonically with an increase in the selling price of hydrogen because the number of hours when the hydrogen market is profitable increases. However, for a given selling price of hydrogen, the optimal capacity factor does not change with an increase in the capacity of the electrolyzer. This shows that the capacity factor of the electrolyzer cannot be assumed a priori as in the case of traditional techno-economic analysis but needs to be optimized

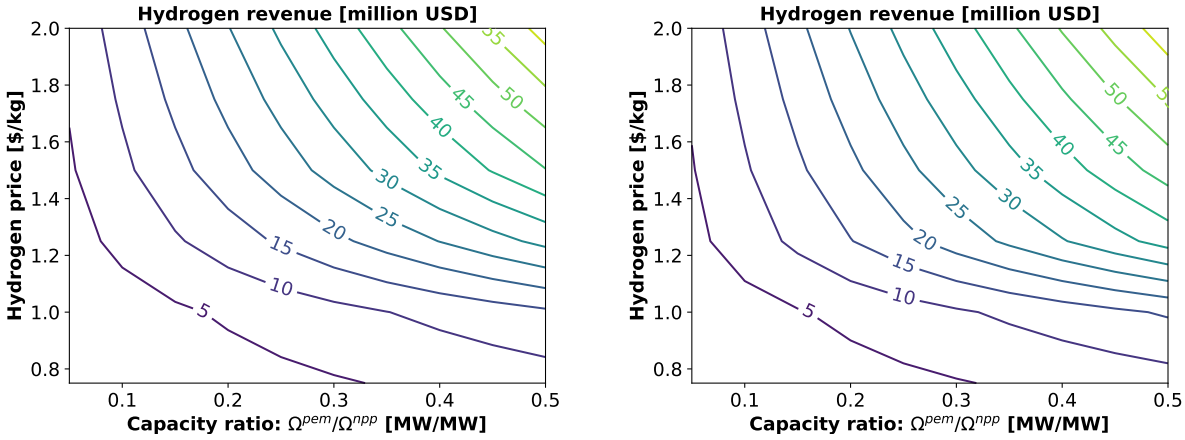

(a) **V1**: Use only DA price

(b) **V2**: Use only RT price

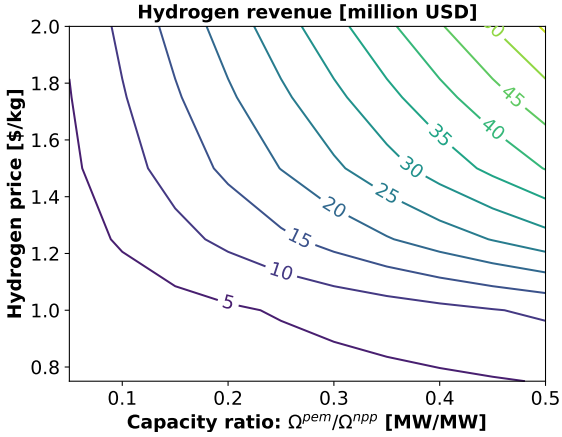

(c) **V3**: Use max{DA, RT} price

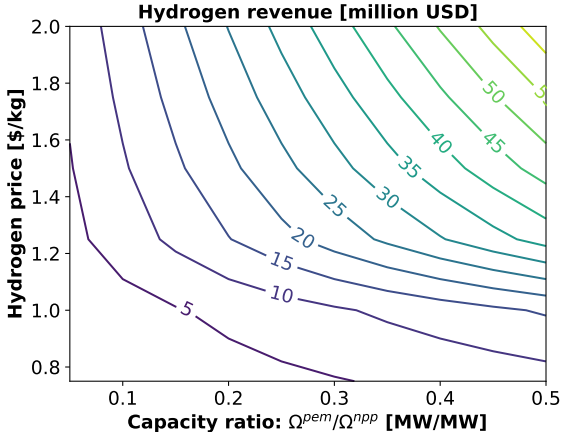

(d) **V4**: Two-step Approach

Figure 2.5: Hydrogen revenue predicted by different price-taker variants.

for a given electricity market. Next, we observe that the optimal capacity factor obtained with **V2** and **V4** is the same, but it is higher than that obtained with **V1** and **V3**. In **V3** the electricity market is more profitable, so the electrolyzer operates less frequently, which explains the lower capacity factor.

To summarize, the key conclusion obtained with the price-taker approach depends on which of the four variants is used. In this case study, with **V1**, **V2**, and **V4**, we conclude that there is a threshold selling price of hydrogen above which participating in the hydrogen market is profitable. However, the threshold selling price of hydrogen obtained with **V1** and **V2** ($1.8/kg) is higher than that obtained with **V3** ($1.2/kg). With **V3**, we conclude that hybridizing the nuclear generator is not economical provided that the selling price of hydrogen is less than $2/kg.

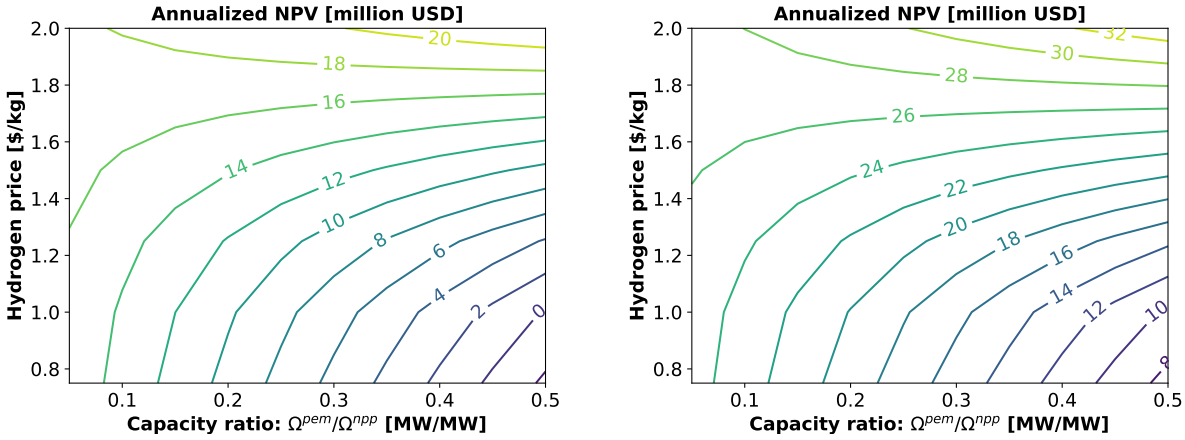

(a) **V1**: Use only DA price

(b) **V2**: Use only RT price

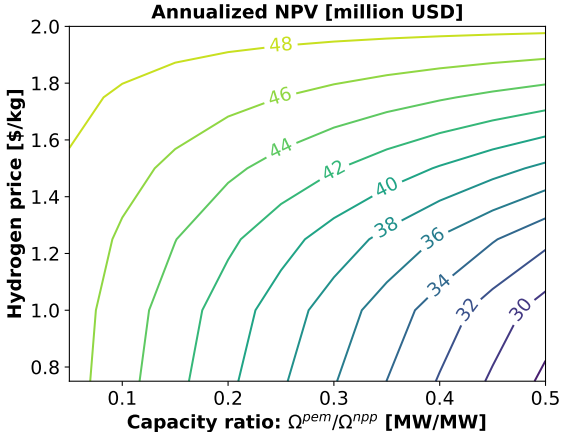

(c) **V3**: Use max{DA, RT} price

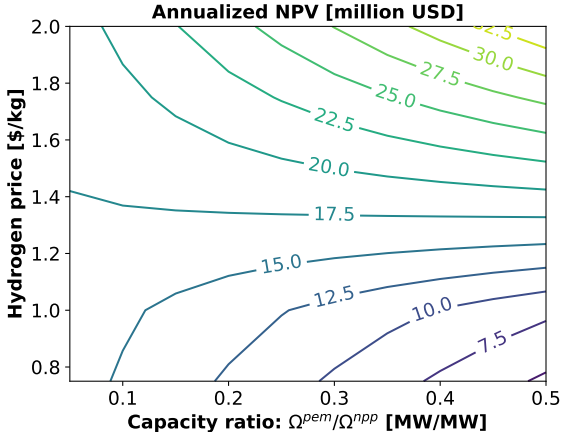

(d) **V4**: Two-step Approach

Figure 2.6: Annualized NPV predicted by different price-taker variants

2.4.2 Results: Validation of Market Surrogates

We construct neural network-based surrogate models for the total revenue and dispatch as described in steps **MS1** and **MS2** in Section 2.3.3. We train neural networks using `TensorFlow-KERAS v2.9.1` [39]. We use two hidden layers each containing 25 nodes, and each node uses hyperbolic tangent (tanh) as the activation function. Figure 2.8 shows the parity plots comparing the data predicted by the surrogate models and the true data. The R^2 value in both cases is above 0.99, indicating that the market outcomes predicted by the surrogate models are accurate.

2.4.3 Results: Optimization with Market Surrogates

Here, we formulate and solve the conceptual design problem using market surrogates with objective (2.7a), and constraints (2.7b), (2.7g) – (2.7o), (2.8), (2.9a) – (2.9c), and (2.10). Figure 2.9 shows the revenue from both electricity and hydrogen markets, the annualized NPV, and the optimal

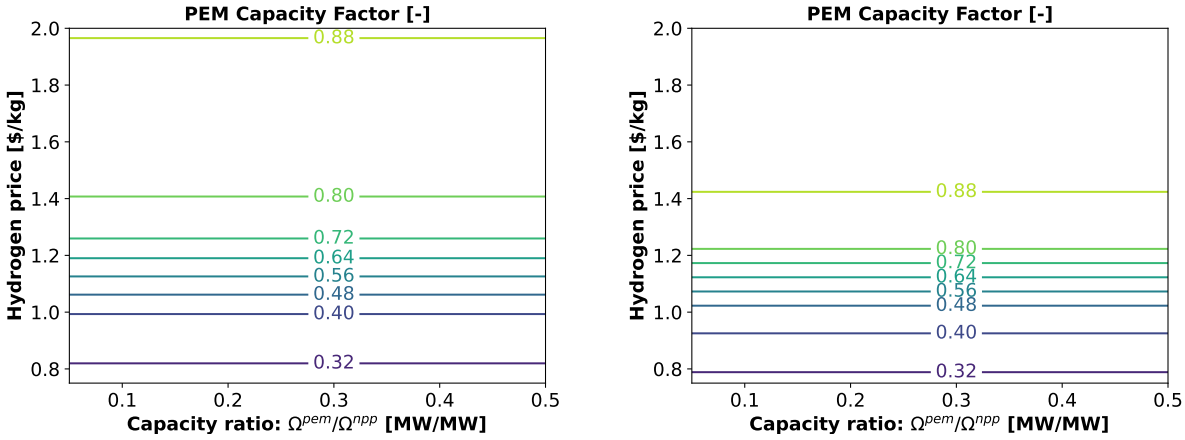

(a) **V1**: Use only DA price

(b) **V2**: Use only RT price

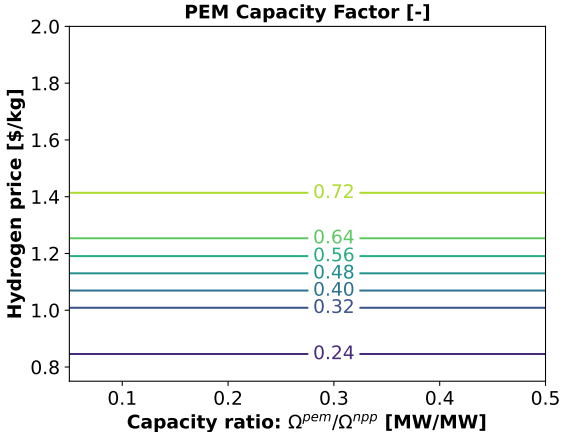

(c) **V3**: Use max{DA, RT} price

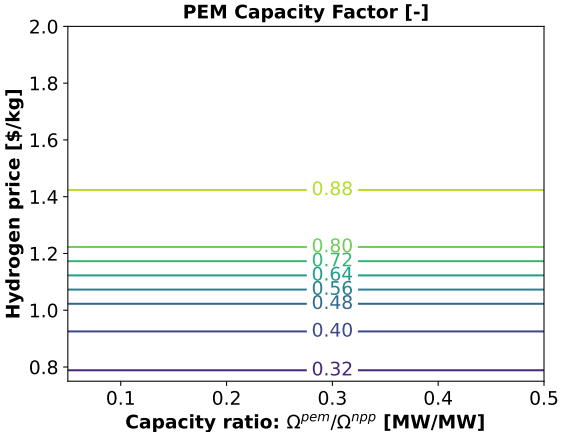

(d) **V4**: Two-step Approach

Figure 2.7: Optimal PEM capacity factor predicted by different price-taker variants

capacity factor of the electrolyzer obtained with the market surrogates approach. We observe that there is a threshold selling price of hydrogen (roughly $1.4/kg) above which participating in the hydrogen market is profitable (see Figure 2.9(c)).

Comparison with the Price-taker Approach

We make the following observations from comparing the results obtained with both the price-taker and market surrogates approaches:

1. The electricity revenue trend obtained with **V1**, **V2**, and **V3** is different compared to that obtained with the market surrogates approach. There exists a range of selling prices of hydrogen between which the revenue from the electricity market increases with an increase in the electrolyzer capacity. The revenue predicted with the two-step variant, **V4**, agrees qualitatively with the more rigorous market surrogates approach. This shows that the new price-taker

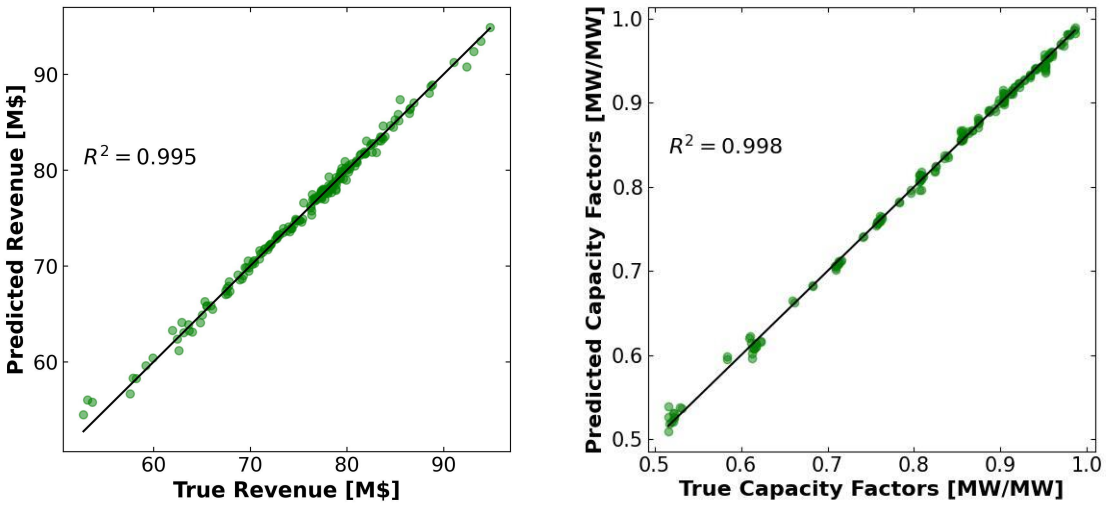

(a) (b)

Figure 2.8: Validation of market surrogate models: (a) the total revenue received by the nuclear generator from the electricity market, (b) fraction of power produced by the nuclear generator that is sold to the grid.

variant developed in this work is potentially an improvement over the existing price-taker approaches. Nevertheless, **V4** overestimates the revenue from the electricity market for higher values of the capacity of the electrolyzer and the selling price of hydrogen.

2. The revenue from the hydrogen market predicted with the market surrogates approach agrees more closely with all four variants of the price-taker approach. But, in terms of magnitude, all four price-taker variants under-predict the revenue from the hydrogen market.

3. The annualized NPV contours obtained with the market surrogates approach are qualitatively similar to the ones obtained with the price-taker approach. However, the threshold selling price of hydrogen at which the decision to build/not build the electrolyzer changes is around \$1.4/kg, compared to \$1.8/kg and\$1.2/kg obtained with the price-taker approach.

4. In all price-taker variants, the optimal capacity factor of the electrolyzer is invariant with the capacity of the electrolyzer. In contrast, the optimal capacity factor of the electrolyzer obtained with the market surrogates approach varies with the capacity of the electrolyzer.

5. Finally, the market surrogates approach captures the impact on LMPs due to the hybridization of the nuclear generator, but the price-taker approach fails to do so. For example, Figure 2.10 shows the price distribution for both DA and RT markets when the nuclear generator `121_NUCLEAR_1` is retrofitted with a 200 MW electrolyzer and the electrolyzer indifference point is chosen to be \$20/MWh. Comparing Figures 2.3 and 2.10, we observe that the frequency of near-zero LMPs decreases and the frequency of LMPs around \$20/MWh increases for the retrofitted case. This is true for both the DA and RT markets. The price-taker approach assumes that the price distribution remains the same, so it cannot account for the changes in revenue due to changes in LMPs. Whereas, the surrogate model for the revenue (see f^{erev} in

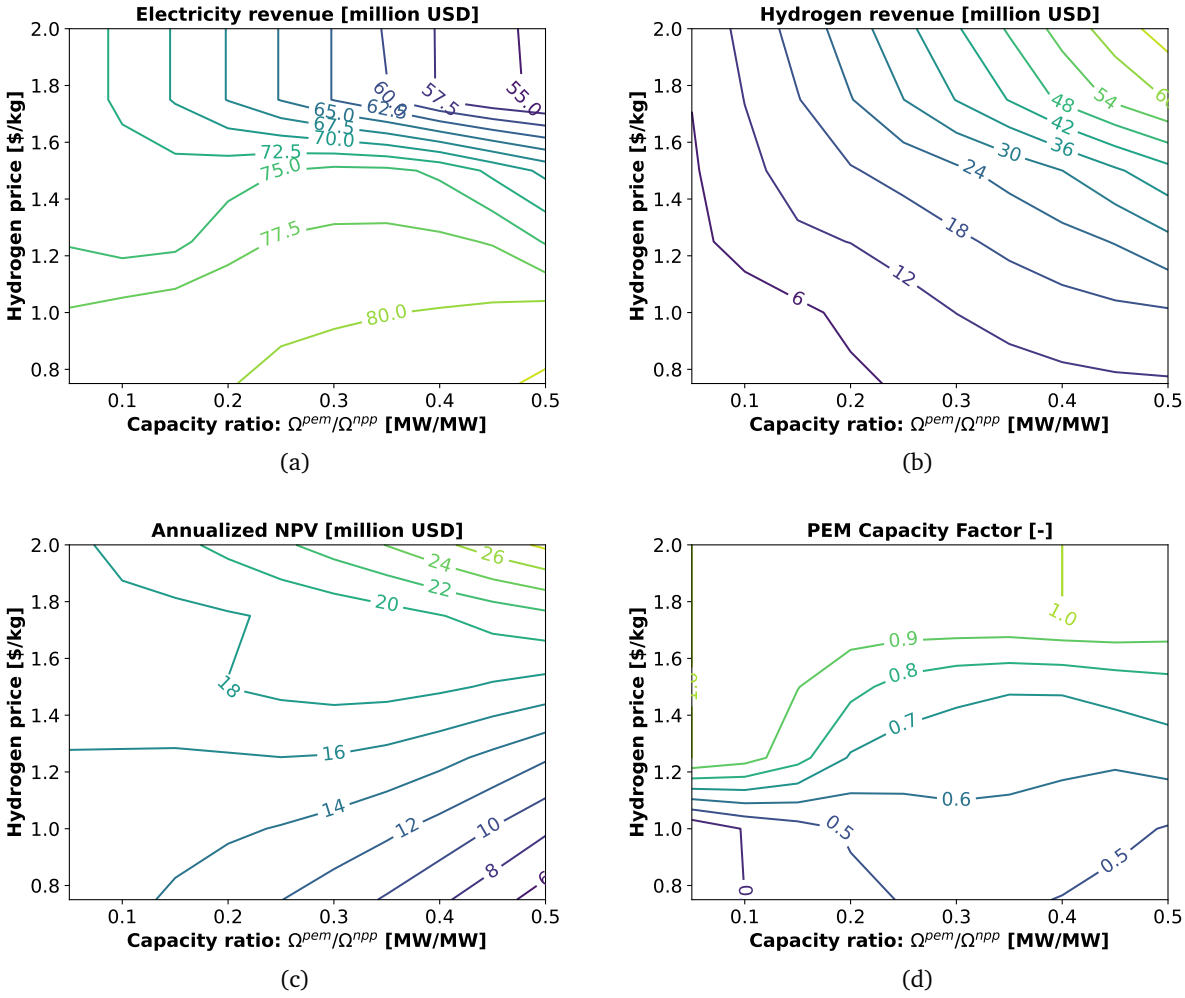

Figure 2.9: Sensitivity of market surrogate results to PEM capacity normalized with the capacity of the nuclear power plant (horizontal axis) and hydrogen price (vertical axis): (a) optimal revenue from the electricity market, (b) optimal revenue from the hydrogen market, (c) optimal annualized net present value, and (d) optimal capacity factor of the electrolyzer.

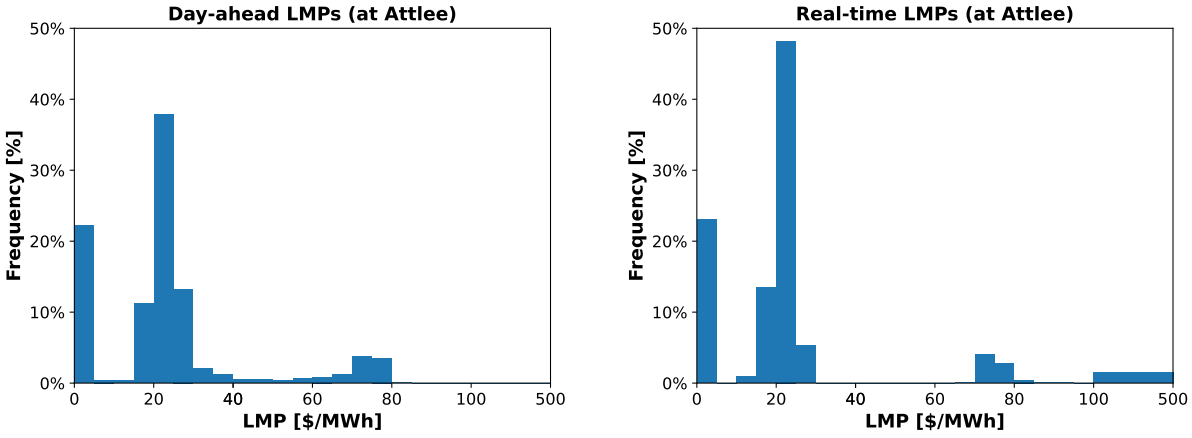

(a) (b)

Figure 2.10: LMP distribution for (a) DA and (b) RT markets at the bus Attlee when the nuclear generator `121_NUCLEAR_1` is retrofitted with a 200 MW electrolyzer, and the electrolyzer indifference point is chosen to be $20/MWh.

(2.7b)) accounts for the impact of the change in LMPs on the overall revenue the generator receives.

2.5 Case Study: Retrofit an Existing Wind Farm

For wind plants to be more responsive to grid conditions and market signals, hybridization with electrolyzers allows participation in the hydrogen market and offers benefits similar to the Nuclear Case Study in Section 2.4. The wind plant is 847 MW, very large relative to the RTS-GMLC system, causing several interesting effects that make hybridization promising. The first is that this wind plant is often curtailed due to excess wind energy and is subject to transmission constraints. LMPs at this 303 bus are relatively low, with 3338 hours having a \$0/MWh RT LMP and the histogram of the LMPs, truncated to \$500/MWh is plotted in 2.14. Second, since the wind plant is so large, forecast errors in the DA vs. RT resource result in expensive penalties and load shed due to penalties from missed DA promises. Due to low LMPs and high penalties, this wind plant in the original RTS-GMLC is not profitable without assuming generous subsidies. Therefore, this case study seeks to improve the value of this wind plant via hybridization with battery or PEM. These wind hybrid plants bid only into the RT market, and not the DA market, to reduce the risk of penalties. So while the price-taker case can use both DA and RT LMPs, the market surrogate case chooses to bid only into the RT market, as in variant **V2** from Section 2.3.2. Because the wind plant already exists, the capital cost of the wind components is not included. However, the O&M costs are. For this case study, there is no depreciation or corporate tax. The existing wind plant bidding only into the RT market has an annual electricity revenue of \$24.5 million and an annualized NPV of \$-10.9 million. Table 2.3 shows the values used for the financial parameters.

Parameter	Definition	Value	Reference
ψ^{pem}	Amount of H_2 produced per unit energy [kg/MWh]	20	[35]
ψ_t^{wind}	Wind capacity factor at time t	$[0, 1]$	RTS-GMLC
γ^{wind}	Overnight capital cost of the wind generator [\$/MW]	1.3×10^6	[40]
γ^{pem}	Overnight capital cost of the electrolyzer [\$/MW]	1.2×10^6	[36]
ϕ_1^{wind}	Fixed O&M cost for the wind generator [\$/MW-year]	4.2×10^4	[40]
ϕ_1^{pem}	Fixed O&M cost for the electrolyzer [\$/MW-year]	$0.03 \times \gamma^{\text{pem}}$	Assumption
ϕ_2^{pem}	Variable O&M cost for the electrolyzer [\$/MWh]	0	Assumption
λ	Lifetime of the plant [yr]	30	Assumption
τ	Corporate tax rate [-]	0%	Assumption
δ	Discount rate [-]	5%	Assumption
ξ	Annualization factor: $(1-(1+\delta)^{-\lambda})/\delta$		
ω	Number of hours in a year	8784	
β^{res}	Reserves as a percentage of total load [-]	15%	Assumption
$\beta^{\text{shortfall}}$	Shortfall price [\$/MWh]	1000	Assumption

Table 2.3: Parameter values used for the renewable case study.

2.5.1 Results: Price-taker Approach

The price-taker design and operation optimization (2.1) was performed for five hydrogen selling prices, ρ^{H_2} = 2, 2.25, 2.5, 2.75 and 3.0 $/kg. Table 2.4 shows the optimal results. The results show that even with the lowest hydrogen price, a small PEM is useful, resulting in an annualized NPV that is $1.4 million larger than that of the original wind plant by diverting the energy from the electricity market with many hours of $0/MWh LMPs to the hydrogen market. As expected, as the hydrogen prices increases, the optimal PEM size also increases, leading to very significant increases in annualized NPVs as the hydrogen revenue increases by up to 5 times while the electricity revenue remains relatively stable, decreasing only 22%. The optimal NPVs are positive only for a hydrogen price of $2.75/kg or higher.

H_2 Price [$/kg]	PEM Size [MW]	H_2 Rev [$mil/yr]	E Rev [$mil/yr]	Ann. NPV [$mil/yr]
2.00	64.7	14.1	21.0	-9.5
2.25	129.9	27.7	19.1	-7.1
2.50	204.0	43.4	17.6	-3.4
2.75	262.2	57.3	16.9	1.4
3.00	322.4	72.0	16.3	7.0

Table 2.4: Price-taker optimal designs from the points sampled for the contour plot

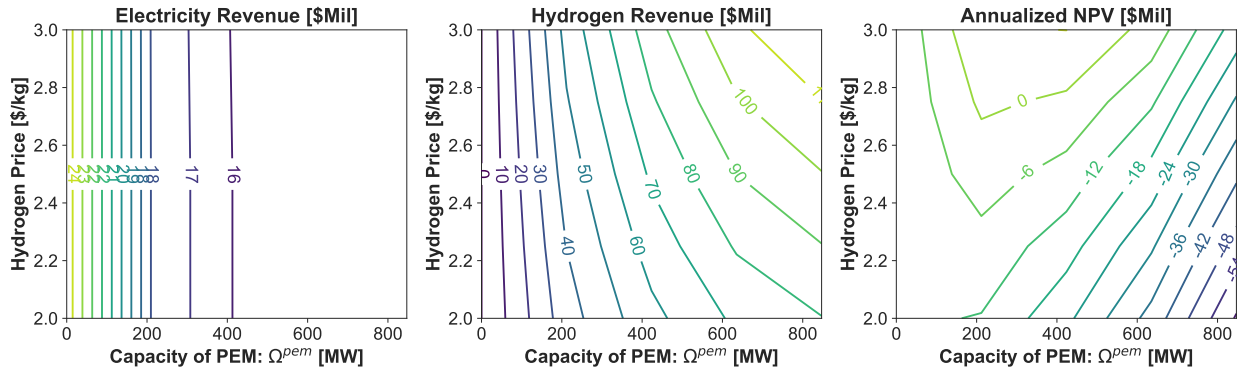

Figure 2.11: Price-taker simulations' contour plot of optimal annualized NPV in million dollars for given hydrogen price and PEM capacity.

Figure 2.11 shows the optimal PEM capacity and NPV for each hydrogen price from running the model as an operation-optimization problem where the size of the PEM is fixed and only the sales decisions are optimized. The 30-year NPVs range from $-683 to $79 million, whereas the annualized NPVs range from $-61 to $7 million. The plots show that the electricity revenue is insensitive to the hydrogen price, which reflects the disconnect between the hydrogen market and the electricity market in this price-taker approach. The $3/kg hydrogen price scenario was selected for comparison with the market surrogate approach below.

2.5.2 Validation of Market Surrogates

The regression performance of the dispatch frequency surrogate is shown in Table 2.5. This shows that the fit of the model to the data was very good and able to capture the capacity factors of each scenario.

	Number of clusters	Mean R^2	Max R^2	Min R^2	STD
Dispatch Frequency Surrogate	20	0.9935	0.9983	0.9774	0.0066

Table 2.5: RE dispatch frequency surrogate regression R^2

We can compare the revenues and NPVs of the surrogate model by sampling at the same design points as the PCM enumeration. Figure 2.12 shows the contour plots of electricity revenue, hydrogen revenue, and annualized NPV for simulations of the system at the points sampled in the Prescient enumeration. For comparison, the contour plots of the simulations using the surrogate model within the NPV-maximization problem to predict revenue and the frequency of each scenario as a function of the PEM bid parameter and the PEM capacity are in Figure 2.13. For both sets of plots, on the left, the electricity revenue contour plot shows how the electricity revenues are highest with a large PEM size and small PEM Bid. As the bid price increases, less energy is sold to the grid. At low bid prices with larger PEM sizes, the electricity revenue increases because more of the energy is sold at a higher price than the original wind bid of $0/MWh, whereas at high bid prices with larger PEM sizes, the revenue decreases because less of the energy clears the market. The second contour plot shows the hydrogen revenue, which, as expected, increases with PEM size and PEM bid since as less energy is accepted by the grid, more of it that goes to hydrogen production.

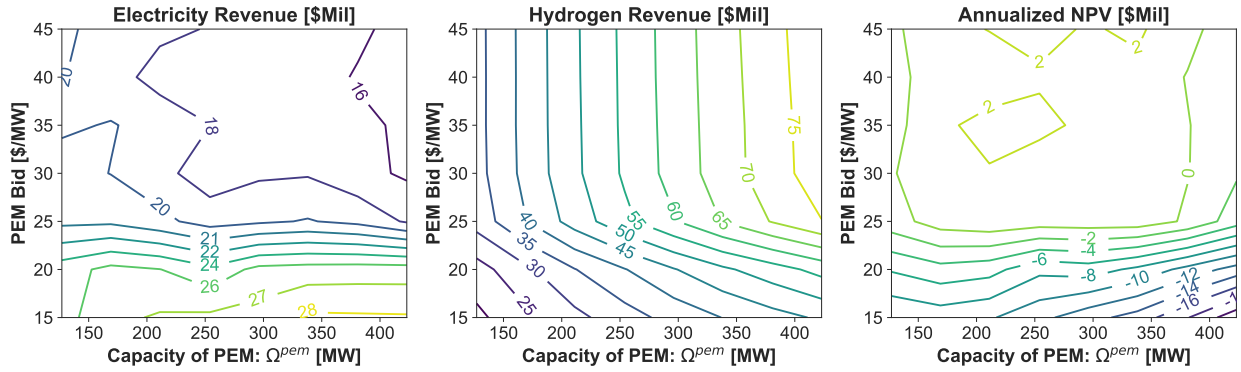

Figure 2.12: Results from PCM enumeration: electricity revenue, hydrogen revenue, and NPVs for designs with various PEM bid prices and sizes

As shown in Figures 2.12 and 2.13, the average percent difference between points in the electricity revenue is -1.5%, with a range of -9.5 to 7.3 %. The average percent difference for the hydrogen revenue is 5.2%, with a range of -2.5 to 2.4%. However, these moderate differences are compounded for the annualized NPV, where the average difference is 13.4%, with a very wide range of percent differences, especially where the PCM enumeration NPVs are close to zero. The highest NPV from the sampled points is about $4.7 million, and the errors range from $-1.6 to $5.42 million.

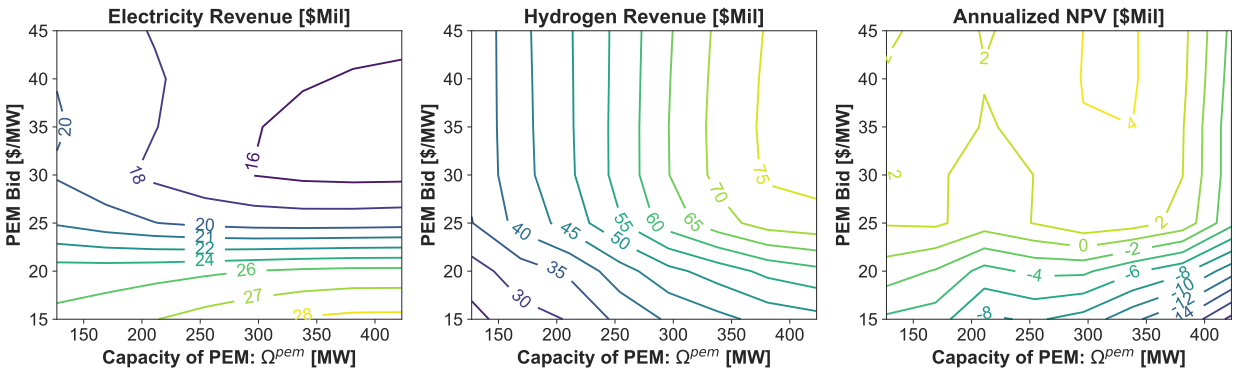

Figure 2.13: Results from surrogate model: electricity revenue, hydrogen revenue, and NPVs for designs with various PEM bid prices and sizes

The comparison between the contour plots in Figures 2.12 and 2.13 shows that despite their high R^2 values, the design optimization problem can compound errors in the dispatch frequency and revenue surrogates. The electricity revenue is purely a function of the revenue surrogate model, so differences in the electricity revenues contours are due to surrogate model itself. The hydrogen revenue is informed by the dispatch frequency model. The electricity and hydrogen revenue contours ranges from 16 to 28 $Mill and 25 to 75$Mill, respectively. Thus the hyrdogen revenue is more influential for the NPV contours.

2.5.3 Market Surrogates Results

The three different optimal design approaches give different results , which are compared in Table 2.6. The price-taker approach gives the largest size (322.4 MW) and has the smallest benefit from participating in the electricity market (17% of revenue), preferring to produce more hydrogen (83%). The PCM enumeration design has the smallest size (211.8 MW) with the highest electricity market revenue (28%) and smallest hydrogen revenue (72%). The market surrogate design has a PEM size (317.4 MW), PEM bid, electricity revenue (20%), hydrogen revenue (80%), and NPV that are between those of the other two designs. Compared to the PCM Enumeration, the Market Surrogate model suggests a 50% larger PEM size and a 70% larger annualized NPV, primarily due to much higher hydrogen revenue. However, the price-taker approach suggests an even larger PEM size (by 52%) and NPV (by 180%). This shows that the market surrogate approach can help bridge the difference between using the full market simulation vs. price-taker time series in design optimization, and produce a design that is closer to the optimum of the full market simulation.

2.5.4 Validation of Optimal Design

To validate the optimal design from the market surrogate approach, the PCM enumeration and market surrogate design were run as a single hybrid thermal-type plant via a Prescient plugin that enables the plant to optimize its bids and dispatch while being simulated within a production cost run in the RTS-GMLC, as described in 2.3.1.

Approach	Optimal PEM size [MW]	PEM Bid [$/MWh]	Electricity Revenue [$mil/yr]	H_2 Revenue [$mil/yr]	Annualized NPV [$mil/yr]
Wind-only	–	–	24.5	–	-10.9
Price-taker	322.4	–	16	79	7
Price-taker Validation	322.4	35	20	68	7.2
PCM Enum.	211.8	35	19	49	2.5
PCM Enum. Validation	211.8	35	20.8	54.1	6.7
Market Surr.	317.4	40.8	16.9	68.1	4.3
Market Surr. Validation	317.4	40.8	19.3	68.0	6.6

Table 2.6: Validation of electricity revenue, hydrogen revenue, and annualized NPV for the market surrogate designs.

Comparing the price-taker against its validation, the latter has a 25% higher electricity revenue and a 14% lower hydrogen revenue, resulting in an annualized NPV of $7.2 million. Comparing the PCM Enumeration against its validation, the latter has a 9.5% higher electricity revenue and a 4.7% higher hydrogen revenue, resulting in an annualized NPV of $6.7 million. Comparing the market surrogate against its validation, the latter has a 14.2% higher electricity revenue and a 0.3% lower hydrogen revenue, resulting in an annualized NPV of $6.6 million. The electricity revenue differences found between the design and its validation are within the expected 10% from different near-optimal solutions to the RTS-GMLC unit commitment problem. However, an important factor for these differences is the reserve participation of the thermal-type validation plant, which results in different dispatch schedules. Despite the differences in PEM size, PEM bid, and predicted versus actual revenues, the difference in annualized NPV between the PCM enumeration validation and the market surrogate validation was only $0.1 million (1.5%), which is much smaller than predicted ($-1.8 million). There may be multiple near-optimal designs within the space, which are suggested by the contour plots of the PCM enumeration results in 2.12. Without sampling the space using the Double Loop framework, it is unclear whether this NPV is close to optimal, but our results show that the market surrogate design has an NPV that is very close to that of the PCM enumeration even though the design is different.

2.6 Conclusions

This chapter demonstrated the conceptual design using market surrogates capability for designing power and hydrogen co-production systems. We demonstrated the capability with two case studies involving an existing generator being retrofitted with a PEM-based electrolyzer for hydrogen production. Participation in hydrogen market couples both the electricity and hydrogen markets, and motivates the need to include market interactions during the design phase. In both case studies, we showed the different optimal designs for price-taker, market surrogates, and PCM enumeration. Both hybrid plants have better financial metrics than the original single-technology plant according to all of the optimal design approaches. Hybridization with PEM gives flexibility to divert energy to the more valuable market and allows plants to operate more responsively to the electricity market,

resulting in improved economics. Regarding the magnitude of NPV increases, our results demonstrated that the classical price-taker approach leads to an incorrect conclusion and sub-optimal designs. The surrogate model approach gives a design that is closer to optimal than the price-taker approach, demonstrating that integrating market interactions is an important component in hybrid design optimization. Our validation of the three different designs in the Double Loop framework shows the importance of plant representation in the PCM, as renewable type or thermal type plants have different properties which lead to different revenues. Creating PCM enumerations and surrogate models using the Double Loop framework would likely improve results, and experiments with derivative-free optimization may also improve optimal design results. The grid-integrated plant modeling and optimization capabilities developed here could be extended to storage and other IESs.

2.7 Appendix

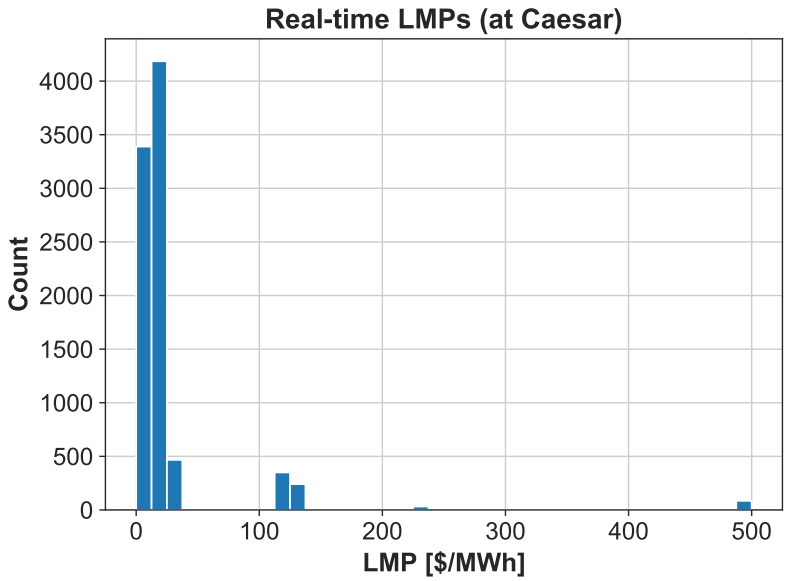

Figure 2.14: Histogram of RT LMPs at the Caesar bus, plot truncated to $500/MWh

Chapter 3

Wind-Battery Hybrid Energy Systems

3.1 Introduction

In recent years, there have been increasing deployments of energy storage systems because of the declining costs of storage technologies and the requirement for renewable energy grid integration. Energy storage has several benefits to the grid, including providing firm capacity, load leveling, and ancillary services [19]. Battery storage is one of the most widely used technologies for energy storage [41, 42]. According to the U.S. Energy Information Administration (EIA), utility-scale battery storage capacity has increased to 7.8 GW as of October 2022 [43]. Battery storage systems exploit the arbitrage in wholesale electricity prices by storing renewable power that would be curtailed during low market price periods and by selling it during high price periods. This process is driven by the difference in electricity prices, where a high price difference will offset the variable costs associated with the charge/discharge cycle, including round-trip efficiency losses [42]. Also, large-scale battery storage systems can help balance peak and off-peak electricity loads and reduce expensive power plant costs at peak load periods.

However, the design and operation of battery storage systems remain a challenge. Although the capital and operating costs are expected to decrease in the future; for example, in 2050, battery OM cost will be 52.5% of that in 2020 [40], the costs of operating a battery storage system are relatively high compared to traditional fossil energy systems [44, 45]. Choosing an appropriate size and capacity for the battery is a critical question that decides the economic performance of the storage system. The dynamic electricity market has fluctuations in price and demand. Thus, it requires an optimal design and operating policy for the battery. If the battery size and capacity are too large, the operator has to pay expensive capital and OM costs for the overbuilt storage system. If the battery size and capacity are too small, the storage system might not provide sufficient storage duration for scenarios like extended outages or prolonged periods of low electricity prices and lose potential opportunities in the electricity market. In this chapter, we retrofit the "`303_WIND_1`" renewable wind farm in RTS-GMLC with a battery storage system. Three questions will be answered in the following sections:

- How does the economic performance improve when hybridizing a renewable power plant with batteries?

- What is the optimal battery design using price-taker approximation and rigorous IES/market multiscale optimization?
- How accurate is the price taker approximation?

3.2 Methods

3.2.1 Problem Statement

We consider the renewable wind and battery storage integrated energy system as shown in Figure 3.1. As the wind farm produces power, the IES can decide to charge the energy storage system by a power of $P_{t,s}^{\text{charge}}$ through the splitter and deliver the rest of the power $P_{t,s}^{\text{split}}$ to the grid. Meanwhile, the IES can also discharge the battery storage system to the grid by a power of $P_{t,s}^{discharge}$. The total amount of power delivered to the grid is $P_{t,s}$, which is a combination of $P_{t,s}^{splitter}$ and $P_{t,s}^{discharge}$ by the mixer. The renewable wind farm that we retrofit in this work is "303_WIND_1" with 847MW maximum power in RTS-GMLC.

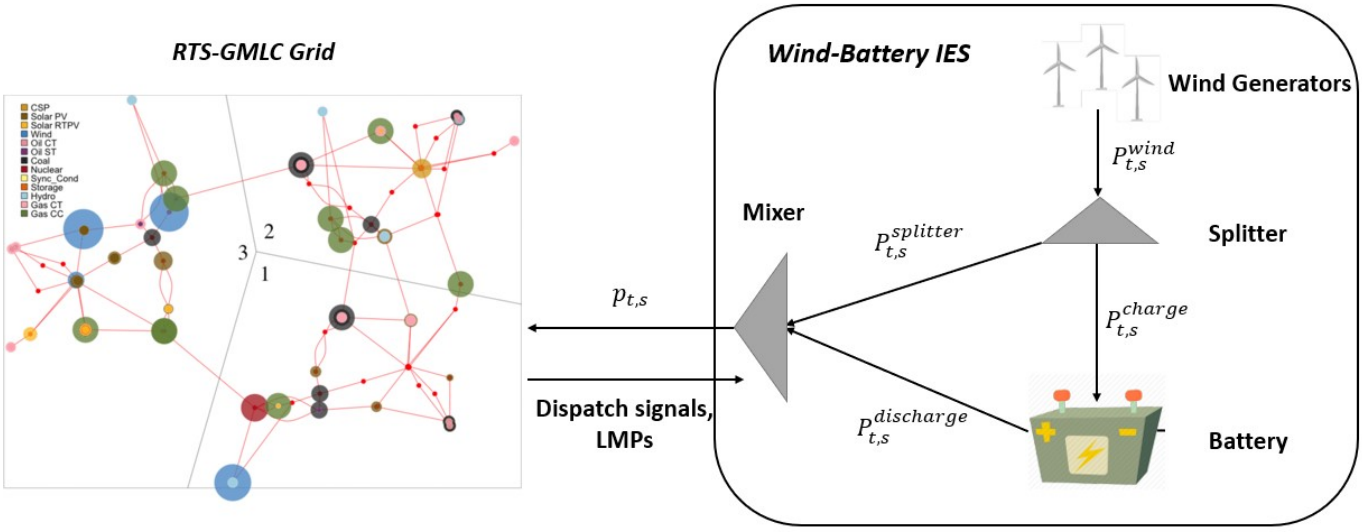

Figure 3.1: Renewable Wind + Battery IES

3.2.2 Price-taker Analysis

The optimization problem (3.1) maximizes the 30-year NPV of the "303_WIND_1" wind power plant and battery storage with different maximum power and capacity. Since we retrofit the "303_WIND_1" wind power plant with a battery storage system with different sizes and capacities, the capital cost of building the wind farm is not included. The price-taker model uses RTS-GMLC synthetic DA and RT LMPs at the "Caesar" bus, generated by PCM using the same parameters as for the nuclear case study (Chapter 2.4), e.g., 15% reserves and a $500/MWh shortfall price. The capital cost and O&M

cost data for the IES are from the NREL database [40]. The price taker optimization model is given as follows (symbols and parameters in the model are listed in Table 3.1):

$$\max \quad NPV \tag{3.1a}$$

$$\text{s.t.} \quad P_t^{\text{wind}} \leq \psi_t^{\text{wind}} \cdot P_{\max}^{\text{wind}}, \quad \forall t \in \mathcal{T} \tag{3.1b}$$

$$E_t - E_{t-1} = (\eta^{\text{charge}} P_t^{\text{charge}} - P_t^{\text{discharge}} / \eta^{\text{discharge}}) \Delta t, \quad \forall t \in \mathcal{T} \tag{3.1c}$$

$$P_t^{\text{charge}}, P_t^{\text{discharge}} \leq P_{\max}^{\text{batt}}, \quad \forall t \in \mathcal{T} \tag{3.1d}$$

$$E^{\text{init}} = E_{\mathcal{T}}, \quad \forall t \in \mathcal{T} \tag{3.1e}$$

$$C_t - C_{t-1} = \frac{1}{2}(P_t^{\text{charge}} + P_t^{\text{discharge}}) \Delta t, \quad \forall t \in \mathcal{T} \tag{3.1f}$$

$$E_t \leq E^{\max} - \sigma C_t, \quad \forall t \in \mathcal{T} \tag{3.1g}$$

$$E^{\max} = S^{\text{batt}} \cdot P_{\max}^{\text{batt}} \quad \forall t \in \mathcal{T} \tag{3.1h}$$

$$P_t^{\text{wind}} = P_t^{\text{charge}} + P_t^{\text{split}}, \quad \forall t \in \mathcal{T} \tag{3.1i}$$

$$P_t = P_t^{\text{discharge}} + P_t^{\text{split}}, \quad \forall t \in \mathcal{T} \tag{3.1j}$$

$$EREV = \sum_{t \in \mathcal{T}} \rho_t^{\text{LMP}} \cdot P_t \tag{3.1k}$$

$$FOM = \sum_{i \in (\text{wind}, \text{batt})} \phi_1^i \cdot P_{\max}^i \tag{3.1l}$$

$$VOM = \sum_{t \in \mathcal{T}} \phi_1^{\text{batt}} \cdot P_t^{\text{batt}} \tag{3.1m}$$

$$CAPEX = \gamma^{\text{batt}} \cdot P_{\max}^{\text{batt}} \tag{3.1n}$$

$$PROFIT = EREV - FOM - VOM \tag{3.1o}$$

$$NPV = PROFIT - (1/\xi) CAPEX \tag{3.1p}$$

The price-taker assumes the electricity grid can take all the electricity from the IES without affecting the LMP. We solve the optimization problem using day-ahead and real-time LMP signals, respectively. The average real-time LMP is \$23.06/MWh, higher than the average day-ahead LMP, \$19.11/MWh, as shown in Figure 3.2. In addition, we use the different capital and fixed-OM cost in 2023 and 2050, which are accessible in Appendix B. With technology advancement, the capital and fixed-OM costs are expected to decrease in the future and as a result, the cost in 2050 will be lower than that in 2023. Using the different LMP signals and costs, we define four scenarios for price-taker optimization parameters.

(DA, 2023): Low electricity price and high capital/fixed-OM cost.

(DA, 2050): Low electricity price and low capital/fixed-OM cost.

(RT, 2023): High electricity price and high capital/fixed-OM cost.

(RT, 2050): High electricity price and low capital/fixed-OM cost.

Parameter	Definition	Value	Reference
ψ_t^{wind}	Wind capacity factor at time t	[0, 1]	RTS-GLMC
η^{charge}	Battery charging efficiency	0.95	Assumption
$\eta^{discharge}$	Battery discharging efficiency	0.95	Assumption
ϕ_1^{wind}	Fixed O&M cost for the wind generator [$/MW-year]	Varies by Scenario	[40]
ϕ_1^{batt}	Fixed O&M cost for the battery [$/MW-year]	Varies by Scenario	[40]
ϕ_2^{wind}	Variable cost for the wind generator [$/MW-year]	0	Assumption
ϕ_2^{batt}	Variable cost for the battery [$/MW-year]	0	Assumption
γ^{batt}	Capital cost of unit power battery [$/MW]	0	[40]
σ	Battery degradation coefficient [-]	0.0001	Assumption
λ	Lifetime of the plant [yr]	30	Assumption
δ	Discount rate [-]	5%	Assumption
ξ	Annualization factor: $(1-(1+\delta)^{-\lambda})/\delta$		
$\mathcal{T}$	Number of hours in a year	8784	

Table 3.1: Parameter values used for the renewable wind-battery price taker optimization.

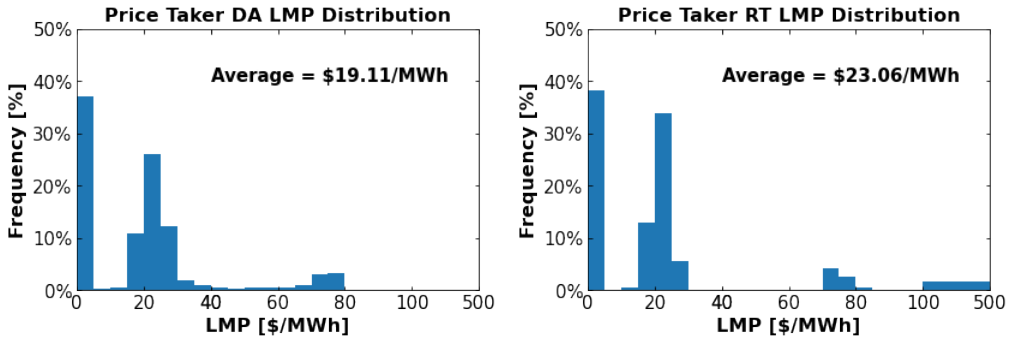

(a) (b)

Figure 3.2: Locational marginal price (LMP) distributions (a) day-ahead market, (b) real-time market from the base case Prescient simulation. These prices are used as the input data for the price-taker optimization.

Typical Battery Storage System Operation Figure 3.3 shows a typical state-of-charge and real-time LMP result of the dynamic nature of the battery storage system. The driving force behind the wind-battery IES profitability is arbitrage in the energy market. The battery is charged during low LMP periods and discharged during high LMP periods.

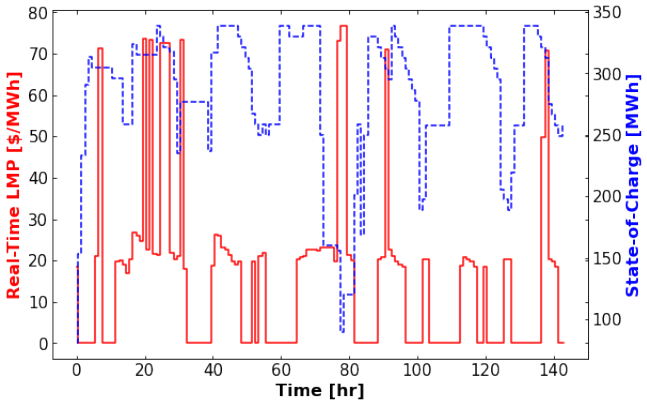

Figure 3.3: Week 1 of Typical battery operation (blue dash) against the real-time LMP (red solid)

3.2.3 Multiscale Simulation Framework

Gao et al. [1] proposed a multiscale simulation framework that integrates the process and grid modeling paradigms to quantify the operational interactions between IESs and wholesale electricity markets. This framework is based on Prescient [24] (PCM) and RTS-GMLC [26] (dataset). As shown in Figure 3.4, there is a day-ahead loop and a real-time loop in the framework. In the day-ahead loop, (a) forecasts of market prices are made within a specific time horizon and (b) the bidder bids the IES into the energy market. Generators can either submit time-invariant bids (static bids) or time-varying bids (dynamic bids). (c) PCM solves unit commitment problems to clear the market. In the real-time loop, (i) PCM solves the economic dispatches problem and gives dispatch signals to each generator. (ii) The generator solves an optimal control problem to track the market signals. (iii) The market calculates settlement payments to each generator. Using the above framework, we can simulate the IES interaction with the wholesale electricity market and analyze its economic performance and electricity dispatch profile. In the bidding step, we can submit time-varying bids to the market to explore different market participation strategies to derive better economic performances.

Dynamic Stochastic Bidder

Optimally operating the wind-battery IES in the dynamic electricity market is challenging. We would like to optimize the IES bids so that the profit is maximized according to the varying market price forecasts. To achieve an optimal operation of the wind-battery IES, at block (b) in Figure 3.4, we propose a stochastic optimization bidding problem [46] that optimizes the battery operation under the electricity market price uncertainty. Solving the stochastic optimization bidding problem,

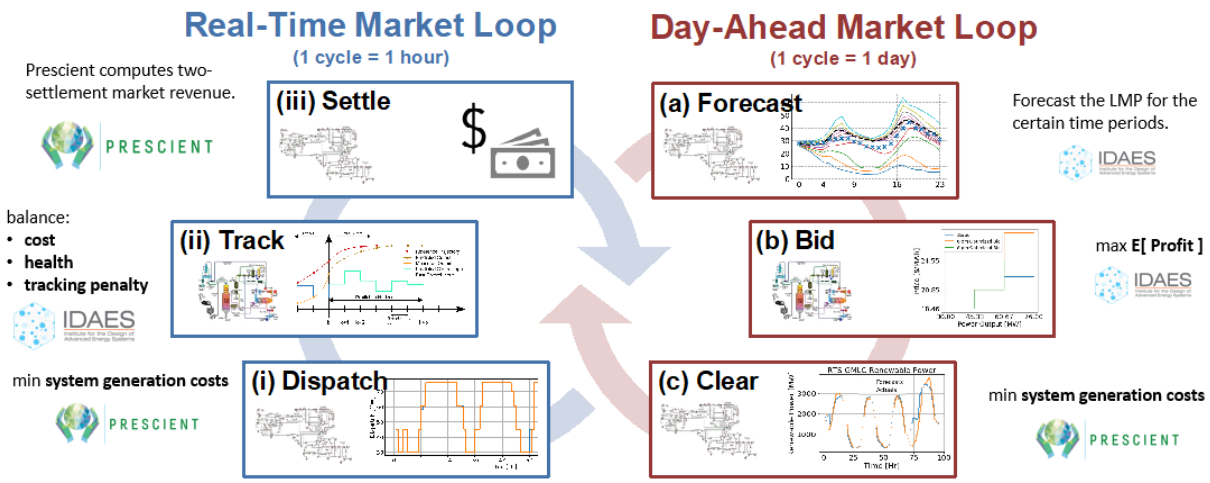

Figure 3.4: Multiscale Simulation framework workflow

the bidder provides optimal time-varying bids for the wind-battery IES in both the day-ahead and real-time markets.

Day-ahead Bidding Problem. On the day before trading, electricity markets allow participating resources to submit their energy bids. In our simulation framework, before the IES solves the day-ahead bidding problems, day-ahead LMPs, along with the corresponding real-time LMPs, are predicted. We implemented a "backcaster" that directly utilizes immediate historical LMPs to construct the day-ahead LMP forecast scenarios $\rho_{t,s}^{DA}$ and the real-time LMP forecast scenarios $\rho_{t,s}^{RT}$. We then use these price forecast scenarios to approximate and maximize the expected profit with the following stochastic program

$$\max \frac{1}{|\mathcal{S}|} \sum_{t\in\mathcal{T}^{\text{DA}},s\in\mathcal{S}} (\rho_{t,s}^{\text{DA}} P_{t,s}^{\text{DA}} + \rho_{t,s}^{\text{RT}}(P_{t,s}^{\text{RT}} - P_{t,s}^{\text{DA}}))\Delta t - c_{t,s} \tag{3.2a}$$

s.t.

$$P_{t,s}^{\text{DA}} \leq P_{t,s}^{\text{RT}} \quad \forall t, s \tag{3.2b}$$

$$P_{t,s}^{\text{RT}} = P_{t,s} \quad \forall t, s \tag{3.2c}$$

$$(P_{t,s}^{\text{DA}} - P_{t,s'}^{\text{DA}})(\rho_{t,s}^{\text{DA}} - \rho_{t,s'}^{\text{DA}}) \geq 0 \tag{3.2d}$$

$$\text{Eq. (3.1b)} - \text{Eq. (3.1h)} \tag{3.2e}$$

Real-time Bidding Problem. Before actual operations, electricity markets allow the resources to submit real-time energy bids to correct deviations from the day-ahead market. At this time, both day-ahead LMP $\hat{\rho}_t^{\text{DA}}$ and day-ahead dispatch level $\hat{P}_t^{\text{DA}}$ have been realized as a result of the day-ahead market clearing. Similarly, the real-time market prices are forecast again with higher accuracy, given less uncertainty.

The underbidding problem is caused by the uncertain nature of the wind resource, where the wind generator fails to meet its day-ahead generation commitments ($\hat{P}_t^{\text{DA}} > P_{t,s}^{\text{RT}}$). To prevent underbidding in the real-time market, Equation (3.3b) provides a relaxed lower bound for the real-time offering power with a slack variable $P_{t,s}^{\text{underbid}}$ for underbidding, which is penalized in the

objective function (3.3a).

$$\max \sum_{t\in\mathcal{T}^{\text{RT}}} \hat{\rho}_t^{\text{DA}}\hat{P}_t^{\text{DA}}\Delta t + \frac{1}{|\mathcal{S}|}\sum_{t\in\mathcal{T}^{\text{RT}},s\in\mathcal{S}} \rho_{t,s}^{\text{RT}}(P_{t,s}^{\text{RT}} - \hat{P}_t^{\text{DA}})\Delta t - c_{t,s} - \omega_t^{\text{RT}}P_{t,s}^{\text{underbid}} \tag{3.3a}$$

s.t.

$$\hat{P}_t^{\text{DA}} \leq P_{t,s}^{\text{RT}} + P_{t,s}^{\text{underbid}} \quad \forall t, s \tag{3.3b}$$

$$P_{t,s}^{\text{RT}} = P_{t,s} \quad \forall t, s \tag{3.3c}$$

$$(P_{t,s}^{\text{RT}} - P_{t,s'}^{\text{RT}})(\rho_{t,s}^{\text{RT}} - \rho_{t,s'}^{\text{RT}}) \geq 0 \quad \forall s, \forall s' \in \mathcal{S} \setminus s, \forall t \in \mathcal{T}^{RT} \tag{3.3d}$$

$$\text{Eq. (3.1b)} - \text{Eq. (3.1h)} \tag{3.3e}$$

In section 3.3.2 to section 3.3.4, we assume the wind-battery IES only participates in the real-time market, and we calculate the multiscale simulation economic values using real-time revenue using Equation 3.4.

$$EREV_t^{\text{RT}} = \rho_t^{\text{RT}} \cdot P_t^{\text{RT}} \tag{3.4}$$

Static Parameterized Bidder

We developed a static parameterized bidder to bid the wind-PEM IES into the energy market. Similar bidding strategies have been proposed in [47, 48] that the PEM-renewable IES bids are formulated based on the forecast electricity price. The parameterized bidder will operate the IES under a fixed strategy given a threshold electricity price, ρ^*. Suppose the predicted electricity price is higher than the threshold price. In that case, IES will offer the maximum available power to make more revenue from the electricity market at the marginal cost of ρ^*. Otherwise, the IES will send the power to PEM and bid the excess energy $\max(P_t^{\text{wind}} - P_{\max}^{\text{pem}}, 0)$. The bid curve of PEM parameterized bidder is given in Figure (3.5).

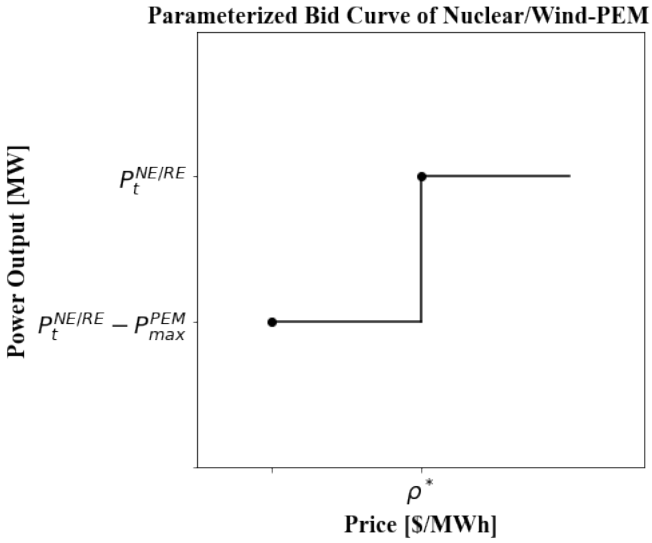

Figure 3.5: When the market price exceeds the critical price ρ^*, the IES bids all the available power into the market. Otherwise, the IES delivers power to PEM as a priority.

3.3 Results and Discussion

3.3.1 Energy storage can improve the economics of wind farms.

We start by comparing the results of three benchmark multiscale simulations of wind generator "303_WIND_1". For these three simulations, the wind generator/IES can bid into both day-ahead (DA) and real-time (RT) markets.

Simulation 1: 303_WIND_1 (847MW), wind generators only.

Simulation 2: 303_WIND_1 (847MW) + 200 MW PEM, use parameterized bidder.

Simulation 3: 303_WIND_1 (847MW) + 50MW (4-hour) battery, use stochastic bidder.

In Simulation 1, we assume wind generators (303_WIND_1) bid the maximum available power at marginal cost = 0, which is the default for the RTS-GMLC dataset. In Simulation 2, using the parameterized bidder, we simulate the same wind generators with a 200MW PEM (see Chapter 2) and set the threshold price $\rho^* = \$25$/MWh. In Simulation 3, we simulate the same wind generators with a 50MW, 4-hour battery storage system.

Most importantly, Table 3.2 shows that if the wind farm is operated independently, it will likely lose a significant amount of money from the real-time market because of the underbidding problem where the real-time power generation cannot satisfy the commitment made in the day-ahead market. However, if the wind generator is operated with a 200MW PEM electrolyzer, the real-time underbidding problem is alleviated if bids for less electricity into the day-ahead market. In the hydrogen market, we assume all the hydrogen can be sold at a price of $3/kg. Under this assumption, although the total electricity revenue is only 4.59M$, the IES received 19.55M$ in hydrogen revenue. Simulation 3 considers the wind + battery IES with different operating strategies. When

	Wind-only	Wind + PEM	Wind + Battery
Bidder	None	Parameterized	Stochastic
Wind Farm Size [MW]	847	847	847
Battery Size [MW]	0	0	50
Battery Capacity [MWh]	0	0	200
PEM Size [MW]	0	200	0
DA Revenue [$M/yr]	17.47	15.76	11.04
RT Revenue [$M/yr]	-19.35	-11.17	14.33
Electricity Revenue [$M/yr]	-1.88	4.59	25.37
Hydrogen Revenue [$M/yr]	0	19.55	0
Total Revenue [$M/yr]	-1.88	24.14	25.37
2023 Wind Farm Fixed-OM cost [$M/yr]	35.39	35.39	35.39
2050 Wind Farm Fixed-OM cost [$M/yr]	28.04	28.04	28.04
2023 Battery Fixed-OM cost [$M/yr]	0	0	1.57
2050 Battery Fixed-OM cost [$M/yr]	0	0	0.84
2023 PEM Fixed-OM cost [$M/yr]	0	7.2	0

Table 3.2: Renewable wind generator benchmark multiscale simulation results

we use the stochastic bidder, we will consider the uncertain scenario of both day-ahead and real-time LMP (i.e., not considering wind generation uncertainty). In such a case, the wind+battery IES achieves 25.37M$ total revenue and is almost as profitable as the wind+PEM IES. Compared with the wind-only simulation, the wind+battery IES significantly reduces underbidding so that we have positive real-time market revenue.

These benchmark simulations show that both hybridization strategies of integrated energy systems are economically viable compared with the wind-only system. Using this framework, we enumerate the different IES design combinations to find the optimal IES design, and we refer to this method as multiscale optimization. In the following sections, we use price-taker optimization and multiscale optimization to optimize the battery storage system. For the remaining parts, we only consider the real-time prices (Equation (3.4)) to avoid low prices and remove the effects of underbidding.

3.3.2 Optimal IES design using price-taker approximation.

To visualize the solution of the price taker optimization in (3.1), we enumerate various combinations of the IES design variables, the battery max power P_{max}^{batt} as a ratio to the max wind farm power P_{max}^{wind} and capacity (hour of battery duration), in the design space. By fixing the IES design and solving for the optimal operation, we obtain the results from Figures 3.6 to 3.8.

Conclusion 1. Using the day-ahead price signal results in the smallest battery design, and the wind-battery IES is not profitable. Figure 3.6(a) and Figure 3.6(b) compare the net present

value (NPV) of wind + battery IES with different battery sizes and capacities using the DA LMP signals. From Figure 3.6(a) and 3.6(b), two plots show the same trend that with the increasing battery size and capacity, the NPV is decreasing. The main reason is that the larger battery size and capacity require more capital and fixed-OM costs, but the marginal return cannot recover the cost of increasing the battery size and capacity. In 2023, the capital and fixed-OM costs are very high, and there will be no positive NPV design. However, in 2050, with the advancement in wind farms and battery technology, lower capital and fixed-OM costs will be available. Thus a positive NPV IES design will be achieved at a small battery size and capacity.

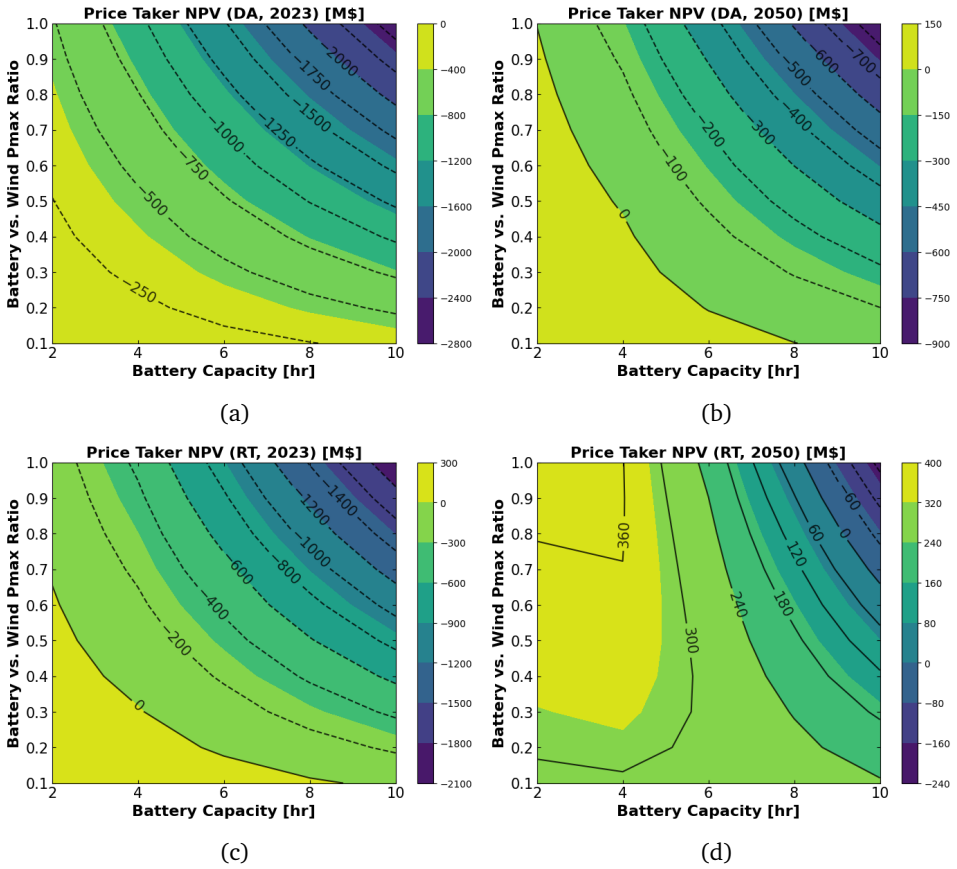

Figure 3.6: Summary of results obtained from price taker optimization: (a) NPV contour plot using DA LMP signal and 2023 cost, (b) NPV contour plot using DA LMP signal and 2050 cost, (c) NPV contour plot using RT LMP signal and 2023 cost, (d) NPV contour plot using RT LMP signal and 2050 cost.

Conclusion 2. Using real-time price signals yields higher NPVs. Figure 3.6(c) and Figure 3.6(d) compare the net present value (NPV) of wind-battery IES using the RT LMP signals. The NPV in Figure 3.6(c) and Figure 3.6(d) is higher than that in Figure 3.6(b) and Figure 3.6(b) because the average RT LMP is about $4/MWh higher than the average DA LMP, and there are some extremely high price periods in RT LMP signals. Because there are no price signal uncertainties in the price taker optimization, the wind-battery IES could achieve the maximum profit at the price spikes. The 2023 cost scenario has the same trend as the day-ahead results, where the price-taker optimization yields the minimal IES design. However, when we consider the 2050 cost scenario, the price-taker optimization gives a different optimal design with the battery maximum power and minimal

capacity (847MW 2-hr battery). This indicates that this IES could be profitable with a lower battery capital and OM cost.

Conclusion 3: The main reason for negative NPV is the high fixed-OM cost for the IES. Figure 3.7 shows the annual profit of the wind-battery IES. A larger battery does not necessarily mean a higher annual profit, as increasing battery size also increases fixed-OM costs. Only when we use high electricity prices and low capital/fixed-OM costs (RT, 2050) does the largest battery capture the highest annual revenue. However, Figure 3.6(d) shows this design has a high capital cost for building the battery storage system and is not economically viable. This finding is consistent with Sorourifar et al. [49], where only trading electricity in the energy market brings a lower return than multiproduct market participation.

Figure 3.7 (e) and (f) shows the electricity revenue from price-taker optimization using DA and RT LMP signals. Both plots indicate the same trend: higher electricity revenue comes with a larger battery. Because price-taker optimization has the perfect information for LMPs and the market can accept all the electricity from the IES, the largest battery can store most electricity at low LMP periods and sell it at high LMP periods. Because the average RT LMP is higher than DA LMP, we have higher electricity revenue using RT LMP signals. Both plots show that the electricity revenue is more sensitive to the battery size than the battery capacity.

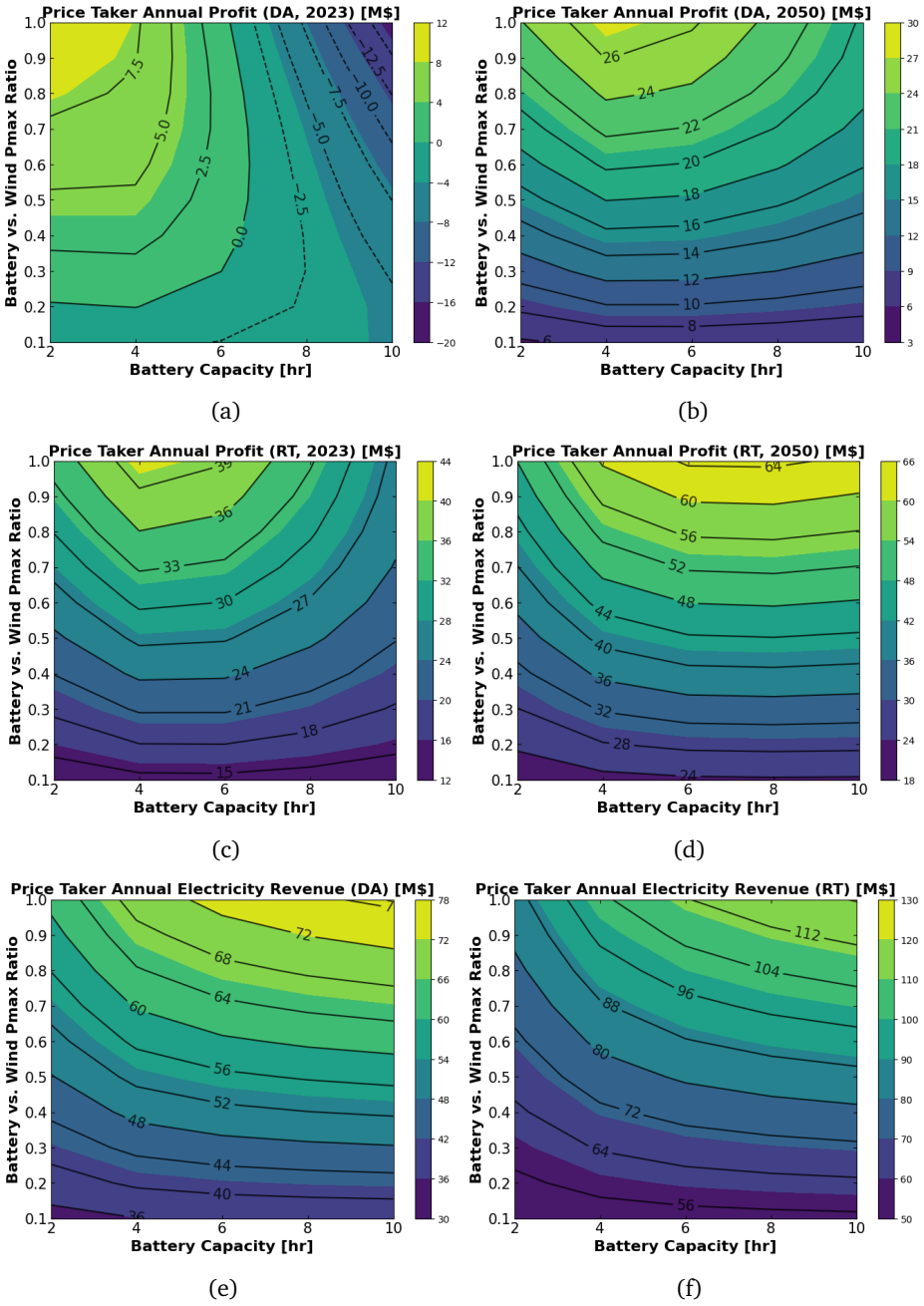

Figure 3.7: Summary of results obtained from price taker optimization: (a) annual profit contour plot using DA LMP signal and 2023 cost, (b) annual profit contour plot using DA LMP signal and 2050 cost, (c) annual profit contour plot using RT LMP signal and 2023 cost, (d) annual profit contour plot using RT LMP signal and 2050 price, (e) annual electricity revenue contour plot using DA LMP signal, (f) annual electricity revenue contour plot using RT LMP signal.

Conclusion 4: Larger battery storage systems reduce the IES renewable curtailments. Figure 3.8 shows the total dispatch and renewable curtailment of wind-battery IES. With the increasing battery size and capacity, less renewable energy is curtailed. The larger battery can store more electricity that should be curtailed at low demand periods and dispatch them to the grid where the

demand is high. Also, we find that the IES curtailment is more sensitive to the battery's maximum power than the battery capacity.

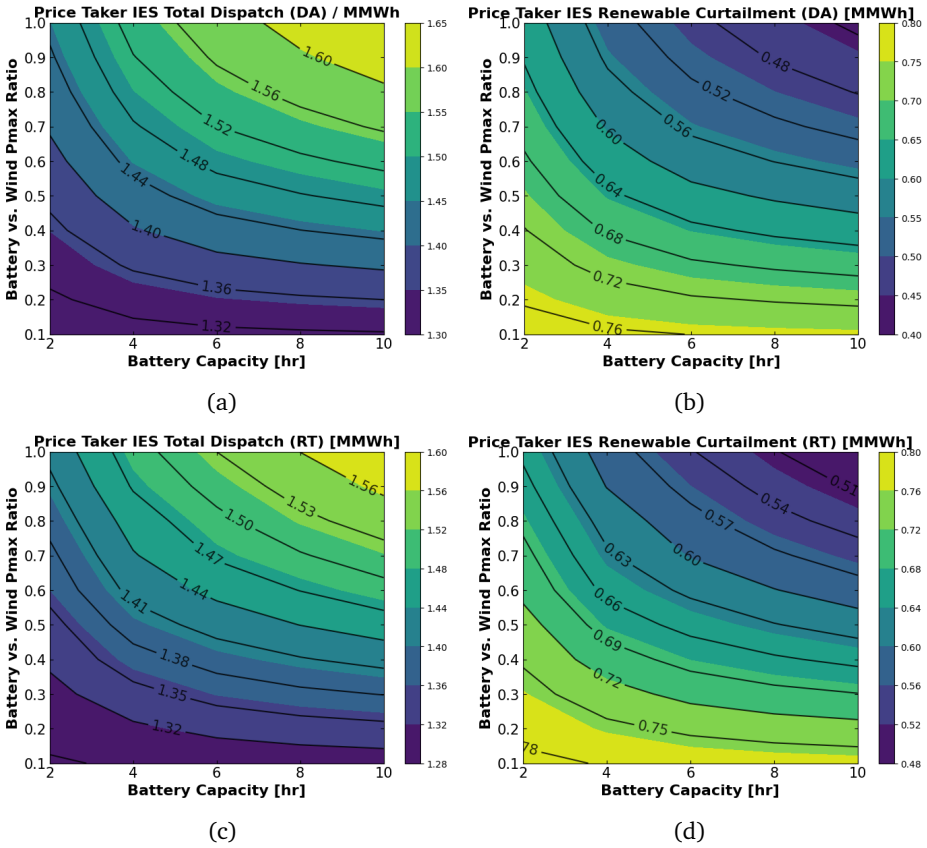

Figure 3.8: Summary of results obtained from price taker optimization: (a) IES total Dispatch contour plot using DA LMP signal, (b) IES renewable curtailment contour plot using DA LMP signal, (c) IES total Dispatch contour plot using RT LMP signal, (d) IES renewable curtailment contour plot using RT LMP signal.

3.3.3 The optimal IES design using the rigorous multiscale optimization.

Next, we enumerate various combinations of the battery max power $P_{\max}^{\text{batt}}$ and capacity in the design space using the multiscale simulation framework to estimate the NPV, dispatch and optimal operating policy.

From Figure 3.9 and Figure 3.10, we find:

Conclusion 5: The wind-battery IES is not profitable when the IES only participates in the real-time energy market. Figure 3.9 (a) and (b) shows the multiscale optimization NPV results using different capital and fixed-OM costs. From the figure, with the increasing size and capacity of the battery, the NPV decreases. NPV results in the multiscale optimization show a trend similar to those in the price taker optimization (3.1). As previously explained, a larger battery system has higher capital and fixed-OM costs. The marginal return cannot cover the marginal cost of increasing battery size and capacity. As a result, NPVs decrease along with the battery size and capacity. Although multiscale optimization NPV results share a similar trend, we find that NPVs are much lower in multiscale optimization than in price taker optimization. The reason is that in multiscale optimization, the electricity revenue and annual profit are much lower than the price taker optimization, as shown in Figure 3.9 (c), (d) and (e). Because the price-taker approximation assumes the grid can accept all electricity from the IES, as we can see in Table 3.3, in the price-taker optimization, more electricity is dispatched to the grid, while the multiscale optimization indicates that this is impossible.

Conclusion 6: The IES has lower electricity revenue with multiscale optimization than with price-taker optimization. Figure 3.9 (e) presents the real-time electricity revenue in multiscale optimization. The average real-time electricity revenue among multiscale optimization is 30.85M$, which is only 38.03% of the price-taker optimization using RT LMP signals (81.11M$). In the multiscale optimization, the stochastic bidder maximizes the expected revenue against uncertain market prices. However, in the price taker optimization, the model has perfect information about market prices (i.e., no uncertainty) and assumes the grid can accept all the electricity without influencing the market prices. In addition, in both problems, the electricity revenue is more sensitive to the battery's maximum power. Even if the battery has a large capacity, the maximum electricity it can discharge within a specific time period is $E_t = P_{\max}^{\text{batt}} \cdot \Delta t$, and the high electricity price period is usually very short (1-4 hours) according to the multiscale optimization. We can observe that the electricity revenue from increasing the battery capacity is not changing significantly, indicating that a large battery capacity is "overbuilt" for the IES because high capital and fixed-OM costs are needed for a large battery.

Case	Market	Average Total Dispatch [MMWh]	Average Renewable Curtailment [MMWh]
Price-taker optimization	RT	1.42	0.66
Multiscale optimization	RT	1.17	0.91

Table 3.3: Comparison of price taker optimization and multiscale optimization IES total dispatch and renewable curtailment.

Conclusion 7: Due to the market interaction between the IES and the grid, in practice, the grid cannot accept as much electricity as the price-taker approximation. Figure 3.10

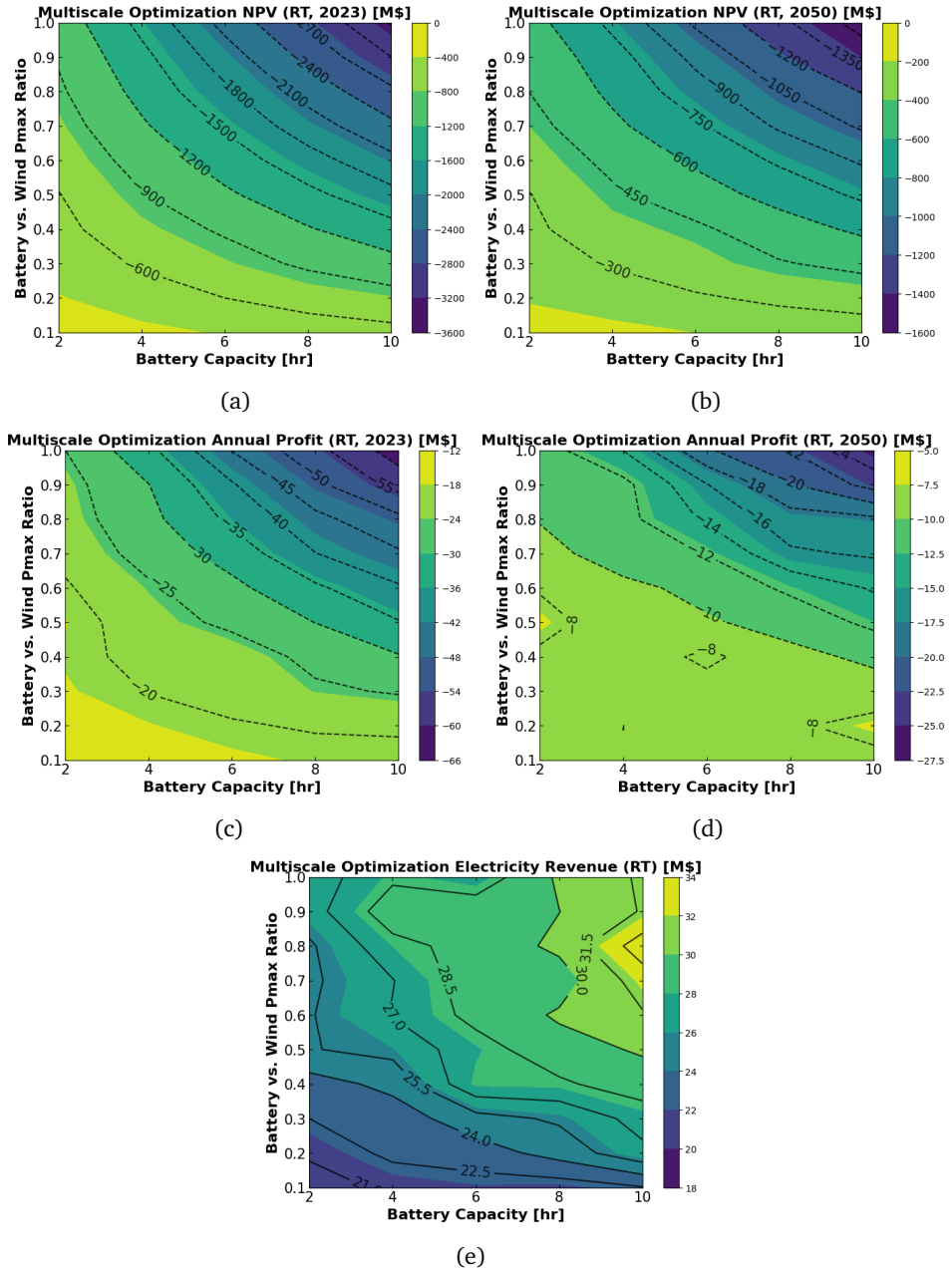

Figure 3.9: Summary of results obtained from the multiscale optimization: (a) 30-year NPV contour plot using real-time revenue and 2023 cost, (b) 30-year NPV contour plot using real-time revenue and 2050 cost, (c) annual profit contour plot using real-time revenue and 2023 cost, (d) Annual profit contour plot using real-time revenue and 2050 cost, (e) annual electricity revenue contour plot using real-time revenue.

shows the wind-battery IES total dispatch and renewable curtailment. The average IES dispatch and curtailment are shown in Table 3.3. Because the price taker optimization assumes the market can accept all the electricity from IES, it has higher total dispatched electricity and lower renewable curtailment. From the multiscale optimization, we find the price taker overestimates the dispatched electricity and underestimates the renewable curtailment. The IES cannot dispatch as much power

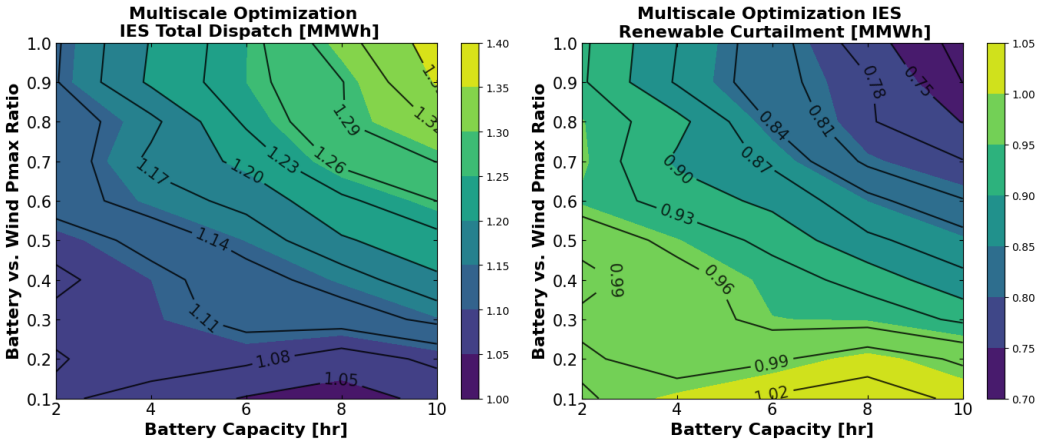

(a) (b)

Figure 3.10: Summary of results obtained from the multiscale optimization: (a) IES total Dispatch contour plot, (b) IES renewable curtailment contour plot.

as the price-taker optimization in a real-world situation.

3.3.4 How accurate is the price taker approximation?

To illustrate the economic viability of retrofitting the wind power plant, we simulate the wind farm-only case in the price taker and multiscale simulation as the benchmark and compare the NPV value of the wind-battery IES with the benchmark. The ΔNPV is calculated in Equation 3.5.

$$\Delta\text{NPV} = \text{NPV}_{\text{IES}} - \text{NPV}_{\text{benchmark}} \tag{3.5}$$

As Figure 3.12 shows, from the price taker optimization, in 2050 (Figure 3.12(b)) we will have positive ΔNPV region, and the optimal design is the battery-wind maximum power ratio of 1.0 and 2-hour capacity. From the multiscale optimization (Figure 3.12(c) and (d)), retrofitting the wind power plant to IES will almost not bring positive returns because of the high costs and low electricity prices in RTS-GMLC. Table 3.4 shows the real-world ISO and RTO historical LMP Data. In RTS-GMLC, the real-time LMP is approximately $23/MWh, which is much lower than the real-world prices as shown in Table 3.4.

	CAISO	ECORT	PJM	NYISO	MISO
Average Real-time LMP (2022, $/MWh)	78.55	64.33	71.25	71.17	61.56
Average Real-time LMP (2021, $/MWh)	43.29	150.39	37.59	35.60	38.28

Table 3.4: ISO average real-time LMP (obtained from: http://www.energyonline.com/Data/)

In Figure 3.13, we compare the wind-battery IES multiscale optimization annual average delta real-time LMP against the price-taker average real-time LMP. As a reminder, the price-taker optimization real-time LMP signals are obtained from the PCM simulation of "`303_WIND_1`" without the

battery storage system. In most simulations, the wind-battery IES interacts with the market and the average real-time LMP is increased at the Caesar bus (where "303_WIND_1" is.). With the higher $P_{\max}^{\text{batt}}$, the IES has higher flexibility to participate in the energy market, and we observe higher delta real-time LMP. To further demonstrate the difference in the real-time LMP distribution, in Figure 3.11, we show (a) the price taker optimization real-time LMP distribution and (b) multi-scale optimization of $P_{\max}^{\text{batt}}/P_{\max}^{\text{wind}} = 0.9$ and battery capacity = 2 hr, real-time LMP distribution. The average real-time LMP in multiscale optimization is 16.6% higher than the price-taker signals, indicating that the IES-gird interaction can significantly impact the market-level data. Also, there are decreasing near zero LMP periods, and instead, more near \$20/MWh LMP periods.

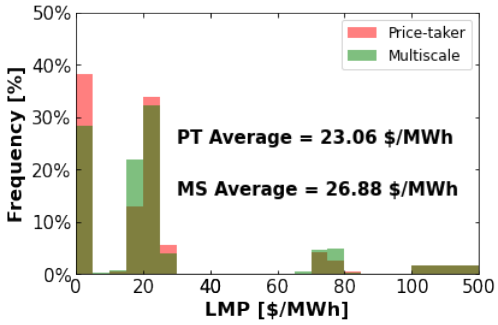

Figure 3.11: Real-time LMP distribution of price-taker optimization and multiscale optimization.

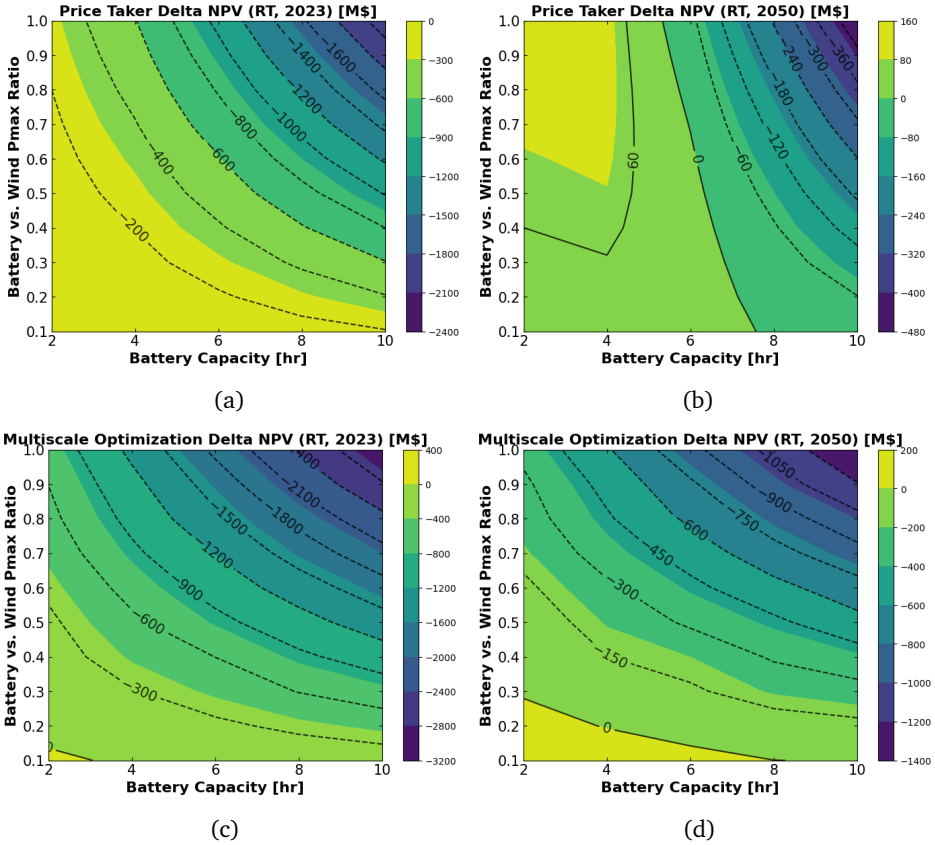

Figure 3.12: Summary of results obtained from price taker optimization: (a) Price taker optimization Δ NPV (RT, 2023), (b) Price taker optimization Δ NPV (RT, 2050), (c) Multiscale optimization Δ NPV (RT, 2023), (d) Multiscale optimization Δ NPV (RT, 2050).

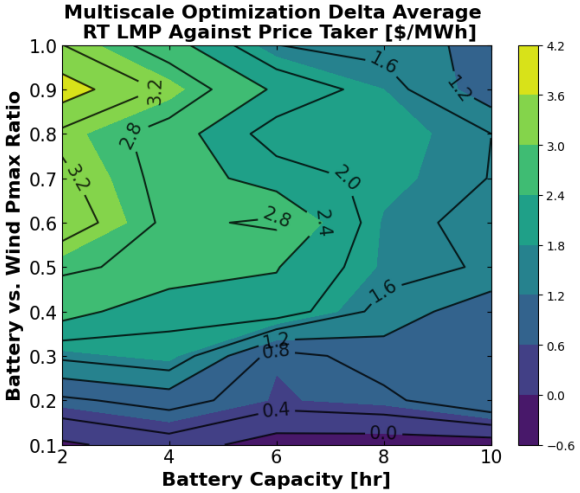

Figure 3.13: Wind-battery IES multiscale optimization annual average delta real-time LMP against price-taker average real-time LMP.

3.3.5 Conclusions and future work

In this chapter, we systematically compared price-taker optimization against multiscale optimization for the techno-economic analysis of a wind-battery integrated energy system.

We find retrofitting the wind farm with the battery storage system (or a PEM) can increase IES flexibility and improve IES profits (Section 3.3.1). The result of the multiscale optimization shows that the IES is approximately 50% less profitable than the price-taker optimization because the grid will not accept as much electricity as the price-taker optimization estimates (Section 3.3.3. Multiscale optimization dispatches 83.4% power of price-taker optimization on average). We find in the multiscale optimization that the IES interacts with the grid and influences market prices, while the price-taker optimization fails to capture these interactions. As a result, it overestimates the IES economic values (Section 3.3.4). Based on the above findings, both the price-taker optimization and the multiscale optimization show that the wind-battery IES can decrease renewable curtailments, but the revenue from the energy market cannot offset the operating costs. In the price-taker optimization, the model ignores the interactions between the IES and grid. However, in the multiscale optimization, we observe the interaction between the IES and the grid through changing market prices, and the grid cannot accept as much electricity from the IES as the price-taker optimization.

As future work, we will apply the surrogate-assisted conceptual design framework shown in Chapter 2 to this wind-battery IES model. We will consider more design variables such as the maximum power of the wind farm. To consider the operational limits of the storage system, we will apply time-series clustering to generate time-series representative dispatch profiles for the stochastic optimization problem. Also, we would like to extend our work to other IESs, such as solar PV, hydro-power, and even IES with more than three technologies. This work proposes a deep insight into the price-taker limitations and enables quantification of IES/grid interaction. In the future, we hope to develop a generalized method to quantify the IES/grid interaction that works for all energy systems instead of being limited to specified models.

Appendix A

Traditional Techno-economic Analysis

Here, we use the traditional techno-economic analysis (TTEA) to determine the optimal size of the electrolyzer for a given electricity market for the nuclear case study (see Section 2.4). The key assumption in the TTEA is that the operation of the system under consideration neither affects nor is affected by the operation of other generators in the grid. For the nuclear case study, this implies that the operation of the electrolyzer is not affected by the grid conditions/requirements and vice versa. Therefore, the capacity factor of the electrolyzer (κ^{pem}) is a degree of freedom, and it can be chosen independent of the grid behavior. To understand the effect of the choice of capacity factor on the overall economics, we perform an analysis with two different arbitrarily chosen values: $\kappa^{\text{pem}} = 0.5$ and $\kappa^{\text{pem}} = 0.75$. (A.1a)–(A.1i) summarize the model for performing TTEA.

$$HREV = (\Omega^{\text{pem}} \cdot \psi^{\text{pem}}) \cdot \mu \cdot \kappa^{\text{pem}} \cdot \rho^{\text{H}_2} \tag{A.1a}$$

$$EREV = (\Omega^{\text{npp}} \cdot \mu - \Omega^{\text{pem}} \cdot \kappa^{\text{pem}} \cdot \mu) \cdot \overline{\rho^{\text{LMP}}} \tag{A.1b}$$

$$FOM = \phi_1^{\text{npp}} \cdot \Omega^{\text{npp}} + \phi_1^{\text{pem}} \cdot \Omega^{\text{pem}} \tag{A.1c}$$

$$VOM = \phi_2^{\text{npp}} \cdot \Omega^{\text{npp}} \cdot \mu + \phi_2^{\text{pem}} \cdot \Omega^{\text{pem}} \cdot \kappa^{\text{pem}} \cdot \mu \tag{A.1d}$$

$$CAPEX = \gamma^{\text{pem}} \cdot \Omega^{\text{pem}} \tag{A.1e}$$

$$DEP = CAPEX/\lambda \tag{A.1f}$$

$$TAX = \max\{0, \tau \cdot (EREV + HREV - FOM - VOM - DEP)\} \tag{A.1g}$$

$$PROFIT = EREV + HREV - FOM - VOM - TAX \tag{A.1h}$$

$$NPV = PROFIT - (1/\xi) \cdot CAPEX \tag{A.1i}$$

The definitions of variables and parameters can be found in Table 2.1. $\Omega^{\text{npp}} = 400$ MW denotes the capacity of the nuclear generator `121_NUCLEAR_1` and Ω^{pem} denotes the capacity of the electrolyzer. (A.1a) and (A.1b) compute the total revenue from the hydrogen and electricity markets, respectively. Here, ρ^{H_2} and $\overline{\rho^{\text{LMP}}} = \$22.09$/MWh denote the selling price of hydrogen and the average locational marginal price at the bus Attlee, respectively. $HREV$ and $EREV$ denote the annual revenue from hydrogen and electricity markets, respectively. (A.1c) and (A.1d) compute the annual fixed operation and maintenance (O&M) (FOM) and variable O&M (VOM) costs for the entire system, respectively. (A.1e) computes the overnight capital expenditure ($CAPEX$) for

installing the electrolyzer. The capital cost of the nuclear generator is not included because we are considering a retrofit of an existing nuclear generator. (A.1f) computes the annual depreciation (DEP) value assuming a straight line depreciation with zero salvage value. (A.1g), (A.1h), and (A.1i) compute the corporate tax (TAX), net profit ($PROFIT$), and the annualized NPV (NPV), respectively.

Figures A.1(a) and A.1(b) (respectively, Figures A.1(c) and A.1(d)) plot the revenue from the electricity (respectively, hydrogen) market for two different capacity factors of the electrolyzer (κ^{pem}), as a function of the ratio of the capacities of the electrolyzer and the nuclear generator ($\Omega^{\text{pem}}/\Omega^{\text{npp}}$) and the selling price of hydrogen (ρ^{H_2}). Figures A.1(e) and A.1(f) plot the annualized net present value as a function of the ratio of capacities and the selling price of hydrogen for $\kappa^{\text{pem}} = 0.5$ and $\kappa^{\text{pem}} = 0.75$, respectively. We make the following observations from these results.

First, the revenue from the electricity market does not vary with the selling price of hydrogen. This is a consequence of fixing the capacity factor of the electrolyzer regardless of the selling price of hydrogen, because of which, the amount of electricity sold to the electricity market is also fixed. However, the revenue from the electricity market decreases with an increase in the ratio of capacities because a higher electrolyzer capacity diverts more power from the electricity market. For the same reason, for a given ratio of capacities, the revenue from the electricity market decreases with an increase in the capacity factor of the electrolyzer (see Figures A.1(a) and A.1(b)). Second, the revenue from the hydrogen market increases with both the selling price of hydrogen and the ratio of capacities. For a given ratio of capacities, a higher selling price of hydrogen yields a higher revenue for the same amount of hydrogen. On the other hand, for a given selling price of hydrogen, a higher ratio of capacities produces more hydrogen, thereby resulting in higher revenue from the hydrogen market. Next, for a given selling price of hydrogen and a given ratio of capacities, the revenue from the hydrogen market increases with an increase in the capacity factor of the electrolyzer (see Figures A.1(c) and A.1(d)). Finally, the annualized NPV decreases with an increase in the ratio of capacities for all values of the selling price of hydrogen in the range \$0.75/kg to \$2/kg. This implies that, for the above range of selling prices of hydrogen, the solution that maximizes the annualized NPV builds the smallest electrolyzer or does not build one at all.

The key conclusion from TTEA is that retrofitting the nuclear generator `121_NUCLEAR_1` is not economical when the selling price of hydrogen is less than \$2/kg.

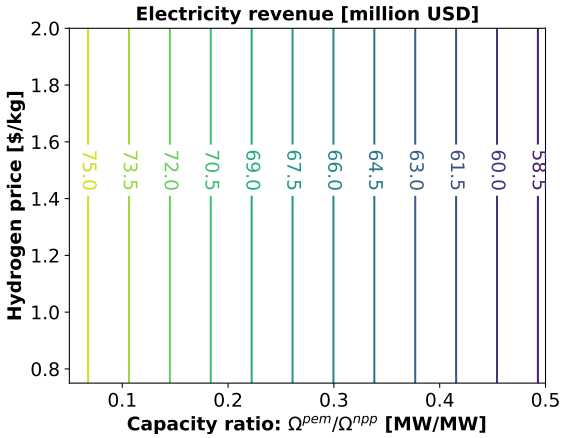

(a) Capacity factor of the electrolyzer = 0.5

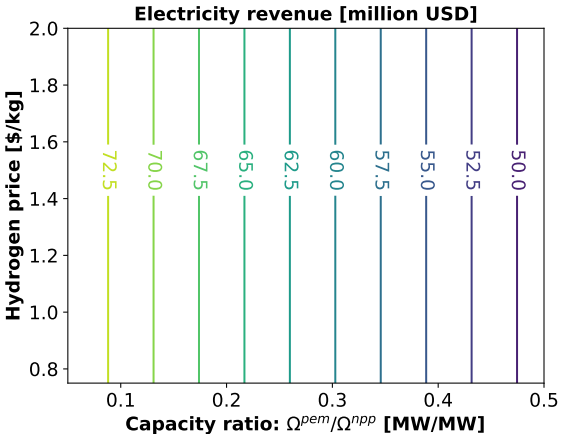

(b) Capacity factor of the electrolyzer = 0.75

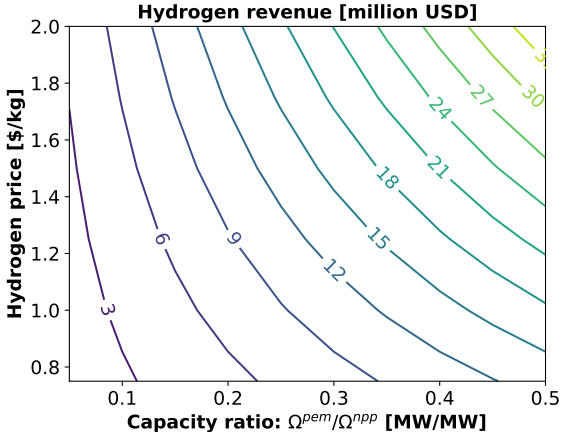

(c) Capacity factor of the electrolyzer = 0.5

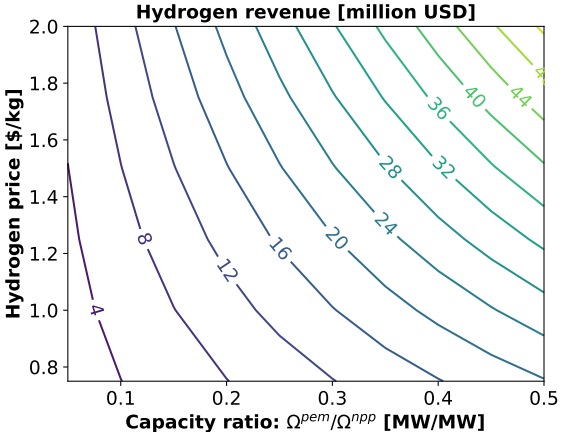

(d) Capacity factor of the electrolyzer = 0.75

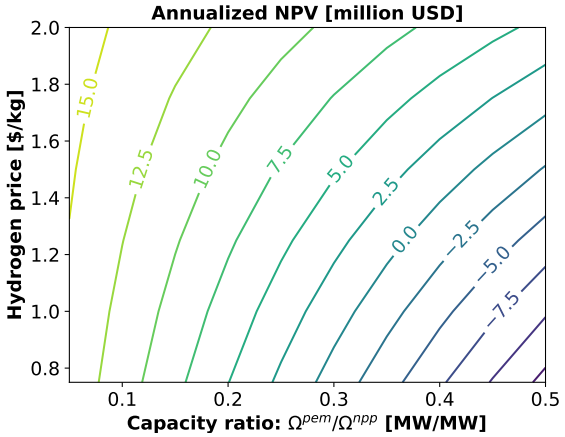

(e) Capacity factor of the electrolyzer = 0.5

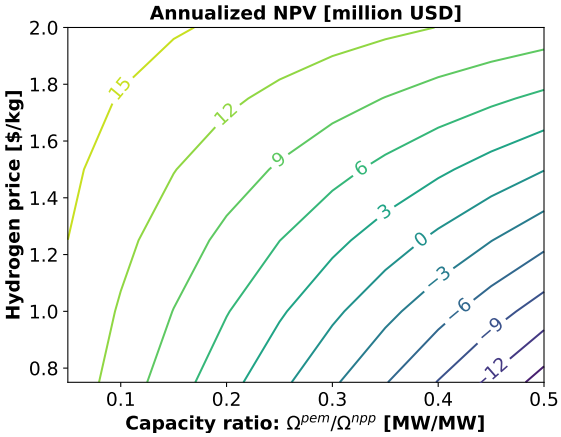

(f) Capacity factor of the electrolyzer = 0.75

Figure A.1: Traditional TEA for the hybridized nuclear power plant as a function of assumed capacity factor of the electrolyzer.

Appendix B

Capital and OM cost data of wind farm and battery storage system

	Wind Farm Capital Cost [$/kWh]	Wind Farm OM Cost [$/kW-yr]
2023	1308	41.78
2050	760	33.108

Table B.1: Capital and OM cost price of wind farms in 2023 and 2050.

	Battery Captial Cost [$/kW]	Battery OM Cost [$/kW-yr]
2023, 2hr	809.46	18.651
2023, 4hr	1353.058	31.39
2023, 6hr	1978.254	44.009
2023, 8hr	2562.651	57.01
2023, 10hr	3147.048	69.618
2050, 2hr	435.108	10.878
2050, 4hr	671.464	16.787
2050, 6hr	907.819	22.695
2050, 8hr	1144.174	28.604
2050, 10hr	1380.53	34.513

Table B.2: Capital and OM cost price of battery storage systems in 2023 and 2050.

Bibliography

[1] X. Gao, B. Knueven, J. D. Siirola, D. C. Miller, and A. W. Dowling, "Multiscale simulation of integrated energy system and electricity market interactions," *Applied Energy*, vol. 316, p. 119017, 2022.

[2] D. J. Arent, S. M. Bragg-Sitton, D. C. Miller, T. J. Tarka, J. A. Engel-Cox, R. D. Boardman, P. C. Balash, M. F. Ruth, J. Cox, and D. J. Garfield, "Multi-input, multi-output hybrid energy systems," *Joule*, vol. 5, no. 1, pp. 47–58, 2021.

[3] A. A. Rahim, A. S. Tijani, S. Kamarudin, and S. Hanapi, "An overview of polymer electrolyte membrane electrolyzer for hydrogen production: Modeling and mass transport," *Journal of Power Sources*, vol. 309, pp. 56–65, 2016.

[4] C. Wang, C. Lv, P. Li, G. Song, S. Li, X. Xu, and J. Wu, "Modeling and optimal operation of community integrated energy systems: A case study from china," *Applied energy*, vol. 230, pp. 1242–1254, 2018.

[5] A. Hajimiragha, C. Canizares, M. Fowler, M. Geidl, and G. Andersson, "Optimal energy flow of integrated energy systems with hydrogen economy considerations," in *2007 iREP symposium-bulk power system dynamics and control-VII. Revitalizing operational reliability*, pp. 1–11, IEEE, 2007.

[6] G. Li, R. Zhang, T. Jiang, H. Chen, L. Bai, H. Cui, and X. Li, "Optimal dispatch strategy for integrated energy systems with cchp and wind power," *Applied energy*, vol. 192, pp. 408–419, 2017.

[7] J. Zheng, J. Chen, Q. Wu, and Z. Jing, "Multi-objective optimization and decision making for power dispatch of a large-scale integrated energy system with distributed dhcs embedded," *Applied Energy*, vol. 154, pp. 369–379, 2015.

[8] J. Zheng, Q. Wu, and Z. Jing, "Coordinated scheduling strategy to optimize conflicting benefits for daily operation of integrated electricity and gas networks," *Applied energy*, vol. 192, pp. 370–381, 2017.

[9] P. Ge, Q. Hu, Q. Wu, X. Dou, Z. Wu, and Y. Ding, "Increasing operational flexibility of integrated energy systems by introducing power to hydrogen," *IET Renewable Power Generation*, vol. 14, no. 3, pp. 372–380, 2020.

[10] F. Ruiming, "Multi-objective optimized operation of integrated energy system with hydrogen storage," *International Journal of Hydrogen Energy*, vol. 44, no. 56, pp. 29409–29417, 2019.

[11] A. Fattahi, J. Sijm, and A. Faaij, "A systemic approach to analyze integrated energy system modeling tools: A review of national models," *Renewable and Sustainable Energy Reviews*, vol. 133, p. 110195, 2020.

[12] C. K. Ekman and S. H. Jensen, "Prospects for large scale electricity storage in denmark," *Energy conversion and Management*, vol. 51, no. 6, pp. 1140–1147, 2010.

[13] I. Gomes, H. Pousinho, R. Melíco, and V. M. F. Mendes, "Bidding and optimization strategies for wind-pv systems in electricity markets assisted by cps," *Energy Procedia*, vol. 106, pp. 111–121, 2016.

[14] Y. Li, W. Xu, X. Zhang, Z. Wang, W. Gao, and Y. Xu, "System value and utilization performance analysis of grid-integrated energy storage technologies in japan," *Journal of Energy Storage*, vol. 63, p. 107051, 2023.

[15] Y. Wang, Y. Zheng, and Q. Yang, "Optimal energy management of integrated energy systems for strategic participation in competitive electricity markets," *Energy*, vol. 278, p. 127883, 2023.

[16] C. Shao, Y. Ding, J. Wang, and Y. Song, "Modeling and integration of flexible demand in heat and electricity integrated energy system," *IEEE Transactions on Sustainable Energy*, vol. 9, no. 1, pp. 361–370, 2017.

[17] F. J. Diaz, J. Contreras, J. I. Muñoz, and D. Pozo, "Optimal scheduling of a price-taker cascaded reservoir system in a pool-based electricity market," *IEEE Transactions on Power Systems*, vol. 26, no. 2, pp. 604–615, 2010.

[18] C. A. Kang, A. R. Brandt, and L. J. Durlofsky, "Optimal operation of an integrated energy system including fossil fuel power generation, co2 capture and wind," *Energy*, vol. 36, no. 12, pp. 6806–6820, 2011.

[19] M. I. Emmanuel and P. Denholm, "A market feedback framework for improved estimates of the arbitrage value of energy storage using price-taker models," *Applied Energy*, vol. 310, p. 118250, 2022.

[20] J. Martinek, J. Jorgenson, M. Mehos, and P. Denholm, "A comparison of price-taker and production cost models for determining system value, revenue, and scheduling of concentrating solar power plants," *Applied energy*, vol. 231, pp. 854–865, 2018.

[21] B. Frew, D. Levie, J. Richards, J. Desai, and M. Ruth, "Analysis of multi-output hybrid energy systems interacting with the grid: Application of improved price-taker and price-maker approaches to nuclear-hydrogen systems," *Applied Energy*, vol. 329, p. 120184, 2023.

[22] RAVEN, "Risk analysis virtual environment," 2023.

[23] A. Lee, J. H. Ghouse, J. C. Eslick, C. D. Laird, J. D. Siirola, M. A. Zamarripa, D. Gunter, J. H. Shinn, A. W. Dowling, D. Bhattacharyya, *et al.*, "The idaes process modeling framework and model library—flexibility for process simulation and optimization," *Journal of Advanced Manufacturing and Processing*, vol. 3, no. 3, p. e10095, 2021.

[24] B. Knueven, J. Ostrowski, and J.-P. Watson, "On mixed-integer programming formulations for the unit commitment problem," *INFORMS Journal on Computing*, vol. 32, no. 4, pp. 857–876, 2020.

[25] M. L. Bynum, G. A. Hackebeil, W. E. Hart, C. D. Laird, B. L. Nicholson, J. D. Siirola, J.-P. Watson, and D. L. Woodruff, *Pyomo–optimization modeling in python*, vol. 67. Springer Science & Business Media, third ed., 2021.

[26] C. Barrows, A. Bloom, A. Ehlen, J. Ikäheimo, J. Jorgenson, D. Krishnamurthy, J. Lau, B. McBennett, M. O'Connell, E. Preston, *et al.*, "The ieee reliability test system: A proposed 2019 update," *IEEE Transactions on Power Systems*, vol. 35, no. 1, pp. 119–127, 2019.

[27] F. Ceccon, J. Jalving, J. Haddad, A. Thebelt, C. Tsay, C. D. Laird, and R. Misener, "Omlt: Optimization & machine learning toolkit," *The Journal of Machine Learning Research*, vol. 23, no. 1, pp. 15829–15836, 2022.

[28] Fair Isaac Corporation, "Xpress optimizer reference manual," 2023.

[29] P. R. Gribik, W. W. Hogan, S. L. Pope, *et al.*, "Market-clearing electricity prices and energy uplift," 2007.

[30] B. Knueven, J. Ostrowski, A. Castillo, and J.-P. Watson, "A computationally efficient algorithm for computing convex hull prices," *Computers & Industrial Engineering*, vol. 163, p. 107806, 2022.

[31] B. Eldridge, R. O'Neill, and B. F. Hobbs, "Near-optimal scheduling in day-ahead markets: Pricing models and payment redistribution bounds," *IEEE Transactions on Power Systems*, vol. 35, no. 3, pp. 1684–1694, 2020.

[32] Gurobi Optimization, "Gurobi optimizer reference manual," 2023.

[33] W. E. Hart, C. D. Laird, J.-P. Watson, D. L. Woodruff, G. A. Hackebeil, B. L. Nicholson, J. D. Siirola, *et al.*, *Pyomo-optimization modeling in python*, vol. 67. Springer, 2017.

[34] A. Wächter and L. T. Biegler, "On the implementation of an interior-point filter line-search algorithm for large-scale nonlinear programming," *Mathematical programming*, vol. 106, pp. 25–57, 2006.

[35] Nel, "PEM Electrolyser M3000 Model," 2023. Accessed: June 8, 2023.

[36] Vickers, James and Peterson, David and Randolph, Katie, "Doe hydrogen and fuel cells program record," 2020. Accessed: June 16, 2023.

[37] Nuclear Energy Institute, "U.s. nuclear operating plant basic information," 2023.

[38] Nuclear Energy Institute, "Nuclear costs in context," 2023.

[39] F. Chollet *et al.*, "Keras." `https://keras.io`, 2015.

[40] N. N. R. E. Laboratory), "2023 annual technology baseline," 2023.

[41] F. Sorourifar, V. M. Zavala, and A. W. Dowling, "Integrated multiscale design, market participation, and replacement strategies for battery energy storage systems," *IEEE Transactions on Sustainable Energy*, vol. 11, no. 1, pp. 84–92, 2018.

[42] J. Bistline, W. Cole, G. Damato, J. DeCarolis, W. Frazier, V. Linga, C. Marcy, C. Namovicz, K. Podkaminer, R. Sims, *et al.*, "Energy storage in long-term system models: a review of considerations, best practices, and research needs," *Progress in Energy*, vol. 2, no. 3, p. 032001, 2020.

[43] "Eia battery capacity in us." `http://https://www.eia.gov/todayinenergy/detail.php?id=54939`. Accessed: 2023-07-27.

[44] W. Cole, W. Frazier, and C. Augustine, "Cost projections for utility-scale battery storage: 2021 update," tech. rep., National Renewable Energy Laboratory, 2021.

[45] U. E. I. Administration, "Electric power annual 2021," tech. rep., U.S. Energy Information Administration, 2021.

[46] X. Gao and A. W. Dowling, "Making money in energy markets: Probabilistic forecasting and stochastic programming paradigms," in *2020 American Control Conference (ACC)*, pp. 168–173, IEEE, 2020.

[47] X. Cheng, J. Lin, F. Liu, Y. Qiu, Y. Song, J. Li, and S. Wu, "A coordinated frequency regulation and bidding method for wind-electrolysis joint systems participating within ancillary services markets," *IEEE Transactions on Sustainable Energy*, 2022.

[48] J. D. Jacobs, *Economic modeling of cost effective hydrogen production from water electrolysis by utilizing Iceland's regulatory power market*. PhD thesis, 2016.

[49] F. Sorourifar, V. M. Zavala, and A. W. Dowling, "Integrated multiscale design, market participation, and replacement strategies for battery energy storage systems," *IEEE Transactions on Sustainable Energy*, vol. 11, no. 1, pp. 84–92, 2020.

www.netl.doe.gov

Albany, OR • Anchorage, AK • Morgantown, WV • Pittsburgh, PA • Sugar Land, TX

(800) 553-7681